



MINISTRY OF AVIATION

AERONAUTICAL RESEARCH COUNCIL
REPORTS AND MEMORANDA

A Wind-Tunnel Investigation of the Directional
and Longitudinal Stability of the *Javelin* Aircraft
at Transonic Speeds, Including Comparison with
Flight Test Results

By E. P. SUTTON and A. STANBROOK

LONDON: HER MAJESTY'S STATIONERY OFFICE

1965

PRICE £1 2s. 6d. NET

A Wind-Tunnel Investigation of the Directional and Longitudinal Stability of the *Javelin* Aircraft at Transonic Speeds, Including Comparison with Flight Test Results

By E. P. SUTTON and A. STANBROOK

COMMUNICATED BY THE DEPUTY CONTROLLER AIRCRAFT (RESEARCH AND DEVELOPMENT),
MINISTRY OF AVIATION

*Reports and Memoranda No. 3403**

December, 1959

Summary.

Directional and longitudinal stability measurements have been made on a 1/72 scale model of the *Javelin* aircraft at Mach numbers up to 1.12 in R.A.E. Bedford, 3 ft Wind Tunnel. Observations were made of the flow over the fin and the wing by the oil-flow technique.

The results show directional instability near sonic speed, as observed in flight, due to shock-induced separation on the fin; this appears to have been caused by the wing trailing-edge shock wave, strengthened by the flow fields of the fin and rear fuselage. A small change in the shape of the rear fuselage delayed the separation to a higher wing incidence and eliminated the instability.

For the model with the tail-on, the curves of pitching moment against normal force had stable slopes except near zero lift at isolated Mach numbers. The stability decreases at high incidence at $M = 0.7$ and at moderate incidences around $M = 0.93$.

Flight and tunnel test results were in good qualitative agreement.

The significant effect of a small distortion of the fuselage shape at the tail (such as might be made to accommodate a supporting sting) on directional stability is of general importance from the point of view of wind-tunnel testing.

LIST OF CONTENTS

Section

1. Introduction
2. Experimental Detail
 - 2.1 Description of the model and balance
 - 2.2 Scope and technique of the tests
 - 2.3 Note on tunnel interference effects
 - 2.4 Accuracy of the results

* Replaces R.A.E. Tech. Note No. Aero. 2563 and Report No. Aero. 2632—A.R.C. Nos. 20 582 and 22 083.

LIST OF CONTENTS—*continued*

Section

Part I Directional Stability

3. Brief Account of the Behaviour of the Full-Scale Aircraft at Transonic Speeds
4. Presentation and Discussion of the Results
 - 4.1 Directional stability and flow over the fin of the basic model
 - 4.2 Effects of modification
5. Comparison with Flight Test Results

Part II Longitudinal Stability

6. Tests Made and Results Obtained
7. Discussion of the Results
 - 7.1 Variation of the lift and moment, and of the flow over the wing, with incidence and Mach number
 - 7.2 Variation of lift-curve-slope and aerodynamic centre with Mach number
 - 7.3 Comparison of aerodynamic-centre position from tunnel and flight tests
8. Conclusions

List of Symbols

List of References

Table 1—Main dimensions of Gloster 'Javelin' model

Illustrations—Figs. 1 to 43

Detachable Abstract Cards

1. *Introduction.*

The tests described here were undertaken primarily to investigate a directional instability near sonic speed observed during flight trails of *Javelin* aircraft. A simple model and a simple balance that could be made quickly were designed for the Royal Aircraft Establishment, Bedford 3 ft Wind Tunnel, and manufactured concurrently with the instrumentation of an aircraft for a flight investigation at R.A.E., Farnborough. The tunnel tests were carried out during July and August, 1955. Additional flight tests were carried out by the Gloster Aircraft Company at Moreton Valence. As far as possible, the tunnel tests were made complementary to the flight tests, which were done at about the same time. In both, particular attention was paid to observation of the flow over the fin, by the surface oil-flow method in the tunnel and by tufting in the flight tests. Minor modifications to the aircraft shape to reduce the yawing tendency were developed. This report deals with the tunnel tests and their contribution to the understanding of the behaviour of the aircraft.

Part I is concerned with the directional stability. A short account of the behaviour of the full-scale aircraft is given first, in Section 3. The results of the tunnel tests on the basic model are presented in Section 4.1 and the effects of various modifications are described in 4.2. The force and angle system used is illustrated in Fig. 1.

Apart from their application to the *Javelin* aircraft, and to other aircraft of similar layout, these tests have two features of more general interest. They afford a comparison between flight experience

and slotted-wall tunnel tests on a model which was a closer representation of the aircraft flow than is usually the case, since aircraft designs are almost always modified between tunnel and flight tests. Secondly, the results cast some light on the effects of distorting the shape of sting-mounted wing-tunnel models near the tail to contain the sting.

Part II gives the results of the longitudinal stability measurements made during the same series of tests together with a comparison with flight test results for the complete aircraft.

2. *Experimental Detail.*

2.1. *Description of the Model and Balance.*

The model represented the *Javelin* Mk. 1 aircraft to 1/72 scale, without flow through the engine ducts. Fig. 2 shows the general arrangement, and the main dimensions are listed in Table 1. A photograph of the model is given in Fig. 3.

The wing was basically of delta planform with a kinked leading edge, the overall sweep being approximately 45° and the aspect ratio 2.91. The wing thickness varied from 10% chord at the root to 7% at the tip. The fuselage was broad and shallow in section, tapering in width from the air intakes, ahead of the wing, to the jet outlet close behind the trailing edge. The tail unit consisted of a large swept fin with a tailplane of approximately delta planform mounted on top of it, forming an endplate. Both fin and tailplane had 9% thick sections. The fin extended well forward of the wing trailing edge.

The intake shape was correctly represented, but there was no flow through the nacelles. Blind ducts from the intakes were bored to a depth of slightly more than two intake diameters. At the tail, the presence of the supporting sting, referred to below, provided partial representation of the jet outflow, and the external fuselage shape was true to scale except in minor details at the jet exit. These details are illustrated in Fig. 4. The modifications which were made in the course of the tests are described in Section 4.2. The longitudinal distributions of cross-sectional area of the basic model and of the model as modified are plotted in Fig. 5.

The wing and body section, made of Tufnol, and the tail unit, made of steel, were attached rigidly by screws to a steel sting which fitted inside the body. For tests with the tail unit off a blanking piece was provided to fill the slot in the fuselage where the tail unit was attached.

The balance was designed in a simple form for quick manufacture, to make tunnel tests possible before the flight tests. Strain gauges were mounted on the sting downstream of the model to measure bending moments from which yawing moment and side force (and for the longitudinal stability tests pitching moment and normal force) were calculated. The shape and surface condition of the sting immediately downstream of the model is indicated in Fig. 4.

2.2. *Scope and Technique of the Tests.*

The tests were carried out in the 35×27 inch slotted working section¹ of the 3 ft Tunnel, R.A.E. Bedford, at Mach numbers between 0.70 and 1.12. Special attention was given to the Mach number range between 0.94 and 1.04.

The total pressure was kept constant at 50 inches of mercury and the temperature at 25°C . The Reynolds numbers based on the aerodynamic mean chord of the wing at $M = 0.70$ and 1.12 were 1.9×10^6 and 2.3×10^6 respectively; the corresponding Reynolds numbers based on the aerodynamic mean chord of the fin were 1.1×10^6 and 1.4×10^6 .

The model and sting could be mounted in the tunnel for tests either at approximately constant incidence over a range of sideslip angle, from -6° to $+5^\circ$, or over a range of incidence at zero sideslip. The sting was cranked so that the angle of incidence at which the model was set for the tests over a range of sideslip was initially about 6° ; the sting was later bent to reduce this to about 2° . The inclination of the model support was measured outside the tunnel and corrections were applied for the bending of the sting due to the normal force and pitching moment on the model. Qualitative observations of the flow over the wing and tail unit were made by means of the surface oil-flow technique.

Boundary-layer transition was fixed on the wings, fin, tailplane and on the fuselage nose throughout the tests by means of carborundum powder suspended in aluminium paint, applied to the model (as shown in Fig. 2). No carborundum was applied to the intake; it was expected that transition would occur close to the lips as a consequence of separation and reattachment of the boundary layer there. The surface oil-flow patterns obtained indicated that the boundary layer had in fact reattached very close to the lip. Surface oil-flow patterns also indicated that there were no sudden extensions of this separated region at high incidence which might otherwise have marked pitch-up effects.

Tests were made on the basic model both complete and without the tail unit, and on the model with the various modifications described in Section 4.2.

2.3. Note on Tunnel Interference Effects.

Measurement of the tunnel Mach number was based on the reference static pressure in the plenum chamber of the slotted working section: no corrections for tunnel wall interference were applied. No corrections for tunnel interference were made to incidence, sideslip, or the measured forces and moments. The errors due to interference may be expected to be small, since the maximum cross-sectional area of the model was only 0.0026 of the working-section cross-sectional area and the span was only 0.25 of the working-section width. However, it should be noted that unpublished work by E. P. Sutton has shown that at near-sonic speeds wall interference tends to delay the rearward movement of strong shock waves with increasing Mach number.

The reflection of the bow wave from the tunnel wall is believed to have passed downstream of the model by a Mach number of 1.05 but at $M = 1.04$ the reflected wave may have impinged on the model with significant effects.

2.4. Accuracy of the Results.

The measurements of the forces and moments were less accurate than is usual in tests of this kind as a consequence of the use of strain gauges on the sting, outside the model, instead of an internal balance. The following table shows standard deviations for the errors of measurement in each force and moment coefficient.

Coefficient	Random error	Total error
C_n	0.0003	0.0005
C_y	0.001	0.0015
C_z	0.004	0.006
C_m	0.003	0.004

Two figures are given for each coefficient. The first represents purely random errors such as the error in reading the strain-gauge balance equipment due to rapid fluctuations of the loads, etc. and indicates the possible scatter from point to point along any curve. The second figure includes the more systematic errors such as those due to the aerodynamic forces on the sting between the strain-gauge stations, 'drift' in the electronic equipment, etc. and indicates the order of magnitude of the absolute error of the measurements.

The angle of incidence and sideslip were measured to about $\pm 0.1^\circ$ in general, but changes in incidence and yaw during any one test were measured to $\pm 0.03^\circ$ or better.

PART I

Directional Stability

3. *Brief Account of the Behaviour of the Full-Scale Aircraft at Transonic Speeds.*

The R.A.E. flight tests of early *Javelin* Mk. 1 aircraft in which the directional instability was investigated were made at altitudes near 40 000 ft. The Mach number range between 0.85 and 1.05 was covered in shallow dives in accelerating or decelerating flight, the lift coefficient varying from a value somewhat below that for level flight (during the entry to the dive) to a value roughly twice that for level flight (during the recovery from the dive). The lift coefficients corresponding to level flight at 40 000 ft are given in the following table.

M	0.90	0.96	1.00	1.04
C_L	0.15	0.13	0.12	0.11

The Reynolds number based on the wing aerodynamic mean chord was of the order of 40×10^6 .

A typical record of a test dive is shown in Fig. 6. The dive was started at 40 000 ft at a Mach number of 0.85 (recording began somewhat later) and speed built up rapidly. There was moderate wing buffeting between $M = 0.925$ and 0.95. At these speeds slight wing dropping occurred but this was easily controlled by the pilot. Between $M = 0.98$ and 0.99 the aircraft yawed to starboard, reaching a maximum angle of sideslip of 4° to 5° at a Mach number of 1.00. This directional disturbance was followed by a normal Dutch-roll oscillation. At speeds between $M = 1.00$ and 1.04 (not reached in the record shown in Fig. 6) the aircraft was quite steady. Recovery was made in a $2g$ pull-out. The various events described for the entry to the dive occurred in reverse order during recovery and were more severe.

In general, the yaw at $M = 0.99$ during both the entry to, and recovery from, the dive could occur in either direction depending on slight asymmetric heading of the aircraft. The yawing tendency was suppressed when the air-brakes were used. The G.A. of the model (Fig. 2) shows the position of the airbrakes, which consisted of slotted rectangular plates at an angle of up to 60° to the wing surface. It was only necessary to extend them to a quarter of their full travel to suppress the yaw.

In the R.A.E. flight tests a ciné-film record was made of the behaviour of tufts on the fin and in the fin-tailplane and fin-body junction. Typical frames from the film are shown in Fig. 7 together

with interpretation of the flow obtained from the complete ciné record*. The shaded areas labelled 'unsteady' and 'very unsteady' indicate regions in which the tufts were oscillating through angles less than and greater than $\pm 60^\circ$ respectively. From Fig. 7b it can be seen that at zero sideslip there were regions of unsteady flow in the fin-tailplane and fin-body junctions, and that over the whole of the rudder the flow was deflected up towards the tailplane. In Fig. 7a, at 4.6° sideslip, it can be seen that on the suction surface of the fin the flow was very steady except in small regions in the junctions, and that very little upward deflection of the flow occurred over the rudder. On the pressure surface there were extensive regions of unsteady flow although it is possible that the rudder deflection was to some degree responsible for this.

4. Presentation and Discussion of the Results.

4.1. Directional Stability and Flow over the Fin of the Basic Model.

Fig. 8 shows the variation of yawing-moment coefficient C_n , with side force coefficient C_Y , for the basic model at various Mach numbers, in most cases for two values of the normal-force coefficient ($-C_z$) in the neighbourhood of 0.1 and 0.4. Figs. 9 and 10 show the corresponding curves of C_n and C_Y against the angle of sideslip, β . Representative curves of the variation of C_n with C_Y , C_n with β , and C_Y with β for the model with the tail unit off are given in Figs. 11, 12 and 13 respectively.

It will be seen from Figs. 8 and 9 that even at the lower Mach numbers the directional stability of the model with the tail unit on is smaller at low angles of sideslip than at the higher angles. The difference becomes more marked at a Mach number of 0.96, and by $M = 0.98$ there is a narrow unstable region near zero sideslip. The instability persists to the highest Mach number of the tests, i.e. 1.12. The width of the unstable region corresponds to 1° or 2° of sideslip and is not symmetrical about the origin (Fig. 9), probably because of some slight asymmetry of the model.

The rate of change of side force with sideslip is smaller in the unstable region than at higher angles of sideslip (Fig. 10). However, the results for the model with the tail unit off (Figs. 11 to 13) show no local reduction in directional stability, nor in the rate of change of C_n and C_Y with β , at low angles of sideslip. Hence it is deduced that the instability is associated with a reduction in the lift-curve slope of the fin. In fact, the effective lift-curve slope of the fin at small angles of sideslip, as estimated from a comparison of the fin-on and fin-off results, becomes negative at Mach numbers above about 0.98.

Fig. 14 shows the variation of $\partial C_n / \partial \beta$ with Mach number for various model configurations. For the model with the tail unit on both the minimum values (attained near zero sideslip) and values at $\beta = -3^\circ$ are shown. This figure shows clearly the change in sign of the contribution of the tail unit at $M = 0.98$. The accuracy of determination of $\partial C_n / \partial \beta$ from the curves of C_n vs. β is poor, particularly for the unstable region, but the values are presented to show graphically the trends described above.

A reason for the loss of fin lift is suggested by observations of oil flow on the fin of the model. Fig. 15 shows surface oil-flow patterns obtained at a Mach number of 1.00 at zero sideslip and a model lift coefficient of 0.14. The photographs show chordwise and slightly downward inclined

* The optical system in the recording apparatus was such that these photographs show mirror images of the actual aircraft.

flow over the forward part of the fin surface, but a mainly upward flow behind a line near mid-chord. The surface is scoured less by the flow over the rear part of the fin. Oil-flow lines on the side of the fuselage are also swept sharply upwards near a line joining the wing root trailing edge to the line of demarcation of the two regions on the fin. On the top of the fuselage aft of this line (not visible in the photographs) the oil is not moved by the flow.

These photographs are interpreted as showing the presence of a strong shock wave across the fin, with boundary-layer separation, or at least severe thickening of the boundary layer, at the foot of the shock wave. It appears that the wing trailing-edge shock wave falls across the fin and is made stronger locally by the increase in supersonic Mach number ahead of it associated with the local expansion caused by the reducing thickness of the fin and the curvature of the rear fuselage. The strength of the shock can be expected to increase with wing lift coefficient, since the strength of the isolated wing trailing-edge shock would increase.

The development and variation of this flow pattern with increasing Mach number is illustrated by Fig. 16. Fig. 16a shows that at a Mach number of 0.90 and a lift coefficient of 0.4 no separation occurs. The boundary layer thickens (reducing the surface shear) and is swept upwards near the trailing edge. Oil-flow observations of the flow over the wing at this lift coefficient show that at this Mach number the wing shock wave is ahead of the fin leading edge (Fig. 37). The lowest Mach number at which there is evidence of a shock wave on the fin at zero yaw at low lift is 0.96. This is shown in Fig. 16b, where a region of sharp upward deflection of the oil streamlines, followed by a recovery towards the chordwise direction, can be seen on the lower half of the fin. The shock position appears to be a little upstream of the wing trailing edge, which would be consistent with observations of the flow on the wing. The photographs for $M = 1.00$ have already been described; the wing shock wave has reached the trailing edge. At Mach numbers of 1.04 and 1.12, Figs. 16d and e, the shock wave appears to lie a little farther back on the fin and to cause separation over the whole fin height; at each Mach number the separation line on the fin can be produced to pass through the wing root trailing edge.

The variation of the pattern with angle of sideslip at a Mach number of 1.00 and a wing lift coefficient of 0.51 is shown in Fig. 17. At small angles of sideslip the shock wave on the pressure side of the fin is slightly downstream of its position at zero sideslip while the shock wave on the suction side is slightly upstream. This is apparent in the photographs for $\beta = 0$ and 1° . There is not much difference between the shock positions for angles of sideslip of 0 and -4° . On the pressure side of the fin at $\beta = -4^\circ$ there appears to be only a local separation at the shock, followed closely by reattachment, over part of the fin height.

It is suggested that the low effective lift-curve slope of the fin for small angles of sideslip at transonic speeds may be associated with the presence, and relative movement, of the shock waves on the two surfaces. The explanation offered is illustrated by the diagrammatic pressure distributions shown in Fig. 18.

Fig. 18a shows, as broken lines, the type of pressure distributions to be expected on the fin at a small angle of sideslip in the absence of any shock waves. The pressure on the suction side of the fin is everywhere lower than on the pressure side. In the Mach number range in which the instability occurs, shock waves are present and cause separation of the fin boundary layer. If the shock waves remained at the same chordwise position with variation of sideslip angle the pressure distribution downstream of the shock waves would be as shown by a full line in Fig. 18a. With separation occurring on both sides of the fin (forming a single bubble which closes downstream of the trailing

edge) there would be very little difference in pressure between the two surfaces downstream of the shock waves. This in itself would account for some loss of lift associated with the presence of the shock waves.

However, it is known from the oil-flow patterns that the shock wave is slightly farther upstream on the suction side of the fin than on the pressure side. In this case, as shown in Fig. 18b, there will be a negative pressure difference across the fin between the shock positions which will give a negative contribution to lift. In certain conditions this could result in a negative effective lift-curve slope; that is, the fin side force could decrease with increasing sideslip angle.

The effective lift-curve slope of the fin recovers again at larger angles of sideslip, presumably owing to a limit being reached in the relative movement of the shock waves.

The significant difference between the flow described here and the case of the isolated aerofoil considered by Pearcey² is that in the present case the shock strength and position are largely determined by aerodynamic components other than the fin itself. In particular, the shock wave is much stronger than any that would have occurred on the isolated fin. The relative movement of the shock waves with varying sideslip will also differ, to some degree, from that on the isolated fin. The explanations of the relative movement with incidence on an isolated aerofoil which are given in Ref. 2 cannot be expected to apply here where the movement with variation of sideslip angle is significantly affected by the flow over the wing and fuselage.

4.2. *Effects of Modification.*

The modifications to the basic aircraft shape which were tested in an attempt to cure the instability are shown in Fig. 19. Their effects on the overall cross-sectional area distribution are shown in Fig. 5. A description and explanation of the purpose of these modifications follows:

(a) The shape and thickness distribution of the fin was altered by an addition to the leading edge over the lower half of the fin span. The fin root chord was increased by 11.8%, the root section thickness was increased to 10.9% of the new root chord, and the position of maximum thickness brought forward to 20% chord. This modification was made by adding a balsa-wood nose to the fin. The surface was coated with 'Phenoglaze' and worked to produce a smooth hard surface, correctly contoured. The object was to test the effect of a simple fin modification which could be expected to slightly reduce the fin contribution to the shock strength.

(b) The upper rear fuselage was modified to increase the cross-sectional area and height at the base and to reduce the streamwise curvature and rate of decrease of cross-sectional area of the fuselage in the neighbourhood of the fin root. This is referred to below as the small rear-fuselage modification. It was built up on the model with balsa wood and 'Plasticene'. It was not made very accurately and its surface was not very smooth. This modification was intended to reduce the shock strength by decreasing the expansion due to the local fuselage curvature upstream of the shock.

(c) A similar but more extensive addition to the rear fuselage, referred to as the large rear-fuselage modification, was obtained by continuing (b) around the sides of the fuselage. This was made of balsa wood, shaped on the model. Again the surface was not very smooth. The dimensions of the added fairing were checked in this case; it was found to be slightly asymmetric and rather flat on the upper surface in cross-section.

(d) A 'bullet' fairing was fitted to the junction of the fin and the tailplane. It was intended to reduce the velocities in the junction of the fin and the tailplane.

(e) Vortex generators were mounted approximately along the quarter-chord line of the fin (as shown in Fig. 19). These were approximately 5% fin chord long and $1\frac{1}{2}\%$ high (approximately 2 boundary-layer thicknesses high). They were set at a spacing of approximately 1.7 generator chords at 30° to the aircraft datum, which resulted in 15° inclination to the surface flow direction given by the oil-flow observation, which was inclined downwards at 15° to the datum. They were constructed from sheet steel 0.002 inch thick and were attached to the fin with 'Araldite'.

Fig. 20 shows the effects of these modifications on the variation of C_n with β at $M = 1.00$ and $-C_z = 0.14$, while Fig. 21 shows the oil-flow patterns on the fin at $M = 1.00$ and $-C_z = 0.2, 0.35$ and 0.5 . The modifications were only tested after the sting had been bent (*see* Section 2.2) and, hence, measurements of yawing moment and side force were only possible at the lowest normal-force coefficient. The vortex generators were applied at an even later stage in the investigation (with the model set so that the incidence could be varied at zero sideslip) and force measurements were not made with this configuration.

It will be seen that the fin root leading-edge extension does not reduce the instability appreciably and that the oil-flow pattern is not changed significantly.

The small rear-fuselage modification reduces the unstable slope of the C_n vs. β curve but the instability is not completely cured. There is a marked alteration in the oil-flow pattern at $-C_z = 0.2$. The oil is still swept up sharply over the rear of the fin but the pattern does not indicate definitely whether separation occurred or not. An oil-flow pattern was obtained at $-C_z = 0.5$ but was not photographed. It showed that separation occurs at this C_z but the extent of separation is less than on the basic configuration.

The large rear-fuselage modification appears to be quite successful at the lowest lift coefficient; the oil-flow patterns show no boundary-layer separation and the force results show only a slight reduction in the stability. This supports the suggestion made in Section 4.1 that the instability is due to a loss of fin lift associated with the separation of the boundary layer on the fin. At the two higher wing lift coefficients the fin boundary layer continues to separate and it is likely that the model is still directionally unstable. As was pointed out in Section 4.1, the contribution of the flow at the wing trailing edge to the shock strength at the fin will increase when the aircraft lift coefficient is increased.

The bullet in the junction of the fin and the tailplane was then tried in combination with the large rear-fuselage modification. The intention was to investigate whether improving the flow in the junction would postpone the instability to higher lift. However, even at the low lift coefficient of the force tests the stability was decreased over a range of sideslip and no improvement could be seen in the behaviour of the boundary layer at the higher lift coefficients.

The oil-flow patterns obtained with the vortex generators on the fin at the two higher lift coefficients suggest that they prevent the separation of the boundary layer. An improvement in stability may be inferred but no force measurements are available to confirm this.

Fig. 22 shows the effect of the modifications on the variation of C_n with β at $M = 1.04$ and Fig. 23 shows some oil-flow patterns obtained at the same Mach number. The results are similar to those obtained at $M = 1.00$ except that the small rear-fuselage modification makes the model just stable.

Since the large rear-fuselage modification cured the instability at $M = 1.00$ and 1.04 (at lift coefficients corresponding to level flight) the force measurements were extended over the whole of the Mach number range in which the basic model was unstable. The results are shown in Figs. 24

to 26. With this modification the model is directionally stable at low lift throughout the Mach number range with only minor reductions in stability near zero sideslip. Curves of $\partial C_n / \partial \beta$ obtained from Fig. 25 are shown in Fig. 14. The values of the slope obtained at $\beta = -3^\circ$ are identical to those for the basic model.

A feature of the results of these tests which is of some general importance from the point of view of wind-tunnel testing is the significant effect on the directional stability produced by a comparatively minor modification to the rear fuselage. It should be noted that, with other configurations, the tailplane contribution to longitudinal stability could be affected in a similar way. Some models may well need to be modified as much as this in order to accommodate an internal strain-gauge balance and sting or to allow flow through the engine ducts to be represented.

5. Comparison with Flight Test Results.

The behaviour of the unmodified aircraft in flight has already been described (Section 3). A comparison between the flight test results and the model results (described in Section 4.1) shows that the directional instability first occurs on the model and the aircraft at approximately the same Mach number. Thus the model shows instability between $M = 0.96$ and 0.98 while the aircraft begins to yaw at a Mach number between 0.97 and 0.98 . At $M = 1.00$, the model tests (Fig. 9) show a possible stable trimmed condition between $\beta = 1\frac{1}{2}^\circ$ and 2° compared with the maximum sideslip angle measured in flight of 4° to 5° . This high peak value recorded in flight is most probably due to the aircraft overshooting the trim value since the damping of these directional oscillations is fairly low. The angles of sideslip obtained later in the dive (between $16\frac{1}{2}$ and 19 seconds, after the damping of the oscillations) are more consistent with the model results. The tuft patterns obtained on the aircraft (Fig. 7) are also consistent with the oil-flow patterns obtained on the model. Fig. 7b may be compared with the oil-flow patterns in Fig. 15. It will be seen that the directions of the tufts are very similar to the local directions of the oil-flow lines.

The aircraft was stable at Mach number between 1.00 and 1.04 but in the model tests the instability persisted throughout the Mach number range up to 1.12 , the limit of the tests. No completely satisfactory explanation of this has been found but it is possible that it is related to the effects of wind-tunnel interference on the rearward movement of shock waves mentioned in Section 2.3.

Only the two rear-fuselage modifications were tested on the aircraft. With the small rear-fuselage modification the aircraft had no tendency to yaw while accelerating during the entry to the dive but there was sometimes a tendency to yaw while decelerating in the recovery from the dive. This could have been due to loss in directional stability at the increased wing lift coefficient experienced during the recovery. Variation in directional stability with lift coefficient may also explain the observed difference in effect of this modification on the model and on the aircraft. In the wind-tunnel tests the model was still unstable but the tests were made at a lift coefficient corresponding to level flight whereas during the entry to the dive the lift coefficient on the aircraft was approximately half this value. Thus it would appear that the small rear-fuselage modification cures the instability at lift coefficients less than about 0.1 . The addition of this modification to the aircraft introduced a limited amount of rudder buffet at low speeds. This was eliminated by the Gloster Aircraft Company during flight development by altering the shape of the extreme rear end of the modified fuselage.

The effect of the large rear-fuselage modification on the stability of the aircraft was similar to that of the small modification. However, increase in fuselage base area had a noticeable effect upon

the performance of the aircraft, and since the small modification was sufficient, flight development of the large modification was not continued.

When the experimental conditions are taken into account, the qualitative agreement which was found between the wind-tunnel and flight observations may be considered to be very satisfactory, at least up to $M = 1.00$. However, it is important to emphasize that the tests might have been completely unsuccessful if the fuselage shape had been changed at the tail, as is often done in aircraft model tests.

PART II

Longitudinal Stability

6. *Tests Made and Results Obtained.*

Measurements of normal force and pitching moment were made at Mach numbers from 0.70 to 1.12 on the basic aircraft model, with and without the tail unit, and on the model with the large rear-fuselage modification with the tail unit on. Axial force was not measured and hence the results are given in terms of the normal-force coefficient, $-C_z$, rather than the lift coefficient. Figs. 27 to 35 show the variation of $-C_z$ and C_m with α and of C_m with $-C_z$ for each of the three configurations.

Oil-flow patterns on the wing surface are shown in Figs. 36 to 39 for Mach numbers of 0.70, 0.90, 0.96 and 1.00. Some of these patterns were obtained with the modified rear fuselage and some on the basic model but it is thought that the modification would have had an insignificant effect except when the wing shock wave was near the trailing edge. In all cases, except $-C_z = 0.56$ at $M = 0.70$ in Fig. 36, the patterns were obtained with the tail unit on, although in most cases it was removed before the pattern was photographed. Except where stated to the contrary, the photographs are of the upper (i.e. suction) surface of the model.

7. *Discussion of the Results.*

7.1. *Variation of the Lift and Moment, and of the Flow over the Wing, with Incidence and Mach Number.*

The variation of lift and pitching moment with both incidence and Mach number followed a similar pattern for each of the three configurations. Consider the results for the model with the tail unit off first (Figs. 27, 28, 29). At $M = 0.70$ the lift varies linearly with incidence up to $-C_z = 0.40$, the moment curve having an unstable slope. With further increase in incidence the lift-curve slope decreases and the stability becomes positive. The oil-flow pattern for $-C_z = 0.38$ in Fig. 36 shows approximately streamwise flow over the major part of the suction side of the wing with approximately spanwise flow near the tips. At $-C_z = 0.56$ the oil-flow pattern shows approximately streamwise flow over the inboard part of the wing (i.e. inboard of the kink) and a spiral flow over the outboard part of the wing. These patterns suggest that the decrease in lift-curve slope and increase in stability above $-C_z = 0.40$ are associated with the onset of a leading-edge separation which originated near the wing tip and moved inboard with increase in incidence.

The oil-flow patterns in Fig. 36 for $M = 0.90$ show considerable differences from those for $M = 0.70$ due to the occurrence of boundary-layer separation induced by the wing shock wave. It first appears at mid chord, approximately 90% semispan, at $-C_z = 0.13$ (and was probably present at somewhat lower lift), and spreads inboard with increase in incidence so that at

– $C_z = 0.20$ the separation occurs over the entire outboard part of the wing (this is clearer on the starboard than on the port wing). For – C_z up to 0.20 the variation of normal force with incidence is linear (Fig. 27) and the stability is constant (Fig. 29); this suggests that the spreading of the extent of separation occurs in a regular way, without rapid large changes within this range of – C_z . Between – $C_z = 0.20$ and 0.30 the lift-curve slope decreases slightly and the stability is increased while the oil-flow patterns show no further development. At – $C_z = 0.39$ the oil-flow pattern (Fig. 37) suggests that the shock wave is farther forward (the pattern is clearer, in this case, on the port wing). The associated increased loss of lift over the rear of the wing results in a reduction of the lift-curve slope and causes an unstable kink in the moment curve. At higher incidences the lift-curve slope and stability recover towards the earlier values.

At $M = 0.93$ and 0.96 the moment curve has an unstable slope for $\alpha < 1.5^\circ$ (Fig. 28). The oil-flow patterns in Fig. 38 for – $C_z = 0.02$ at $M = 0.95$ show boundary-layer separation occurring at the shock waves on both surfaces near zero lift. The unstable moment can be associated with differential movement of these shock waves as the incidence varies, as explained for shock waves on the fin in the investigation of directional stability in Section 4.1. The moment curve has a stable slope from – $C_z = 0.06$ to 0.56 (the maximum tested) apart from a region between – $C_z = 0.30$ and 0.38. The oil-flow patterns in Fig. 38 show a large change in the character of the flow between – $C_z = 0.11$ and 0.42. At – $C_z = 0.11$ the wing shock wave (and the associated separation) is near the trailing edge of the wing and is approximately normal to the incident flow. At – $C_z = 0.42$ separation is seen to occur at a nearly normal shock wave on the outboard part of the wing and at an oblique shock on the inboard part of the wing. It is probable that this change in the flow pattern occurs within the range of – C_z from 0.30 to 0.38 causing the loss of stability shown in Fig. 29 by a reduction in lift over the rear part of the wing.

The oil-flow patterns in Fig. 39 for $M = 1.00$ show a gradual development of the flow with increase in – C_z . At low lift, – $C_z = 0.14$ and 0.19, the flow appears to separate just ahead of the trailing edge on the outer third of the span. With increase of lift, to – $C_z = 0.28$, an oblique shock develops roughly parallel with the inner portion of the leading edge. Where this shock wave meets the trailing-edge shock wave, the separation extends forward slightly from the trailing edge. (The large blobs of oil in these regions are thought to be due to the collapse, during the stopping sequence of the tunnel, of accumulations of oil within the separated regions.) At – $C_z = 0.50$ the pattern has developed further. Separation occurs at the oblique shock over most of the span with separation at a nearly normal shock near the tips. The lift and moment vary linearly with incidence (Figs. 27, 28) in the range tested except for the apparently unstable region near zero lift. Since this is indicated by only one point it should be considered with some reserve.

At $M = 1.04$ and 1.12 the lift and moment curves are linear except for a small region of reduced stability around – $C_z = 0.4$ at $M = 1.04$.

The presence of the tail unit had an appreciable effect on the flow over the inboard part of the wing. Thus, as shown in Fig. 40, for – $C_z = 0.11$ at $M = 0.96$ without the tail unit the wing shock wave is parallel to the trailing edge over the whole span whereas with the tail unit in position the shock wave is farther aft over the inner half of the wing, reaching the root-chord trailing edge. In the latter case smaller areas of the wing are affected by the shock-induced separations and the quantitative effects on the stability are reduced. Thus, for – C_z between 0.3 and 0.4 at $M = 0.90$ and 0.96 the stability decreases with the tail unit off but remains constant with the tail unit on (Figs. 29 and 32). At $M = 1.12$ with the tail unit on there is a slight decrease in stability above

– $C_z = 0.2$ which is not accompanied by a corresponding change in lift-curve slope. This may be caused by a loss of tailplane lift due to forward movement of shock-induced separation on the upper surface of the tailplane.

The addition of the large rear-fuselage modification had only a minor effect (Figs. 33, 34 and 35), producing a small negative increment in $-C_z$ and a small positive (nose-up) increment in C_m . At $M = 0.96$ the unstable region near zero lift extends up to an incidence of 1.5° with the modified rear fuselage (compared with 1.0° for the basic model). This change can be associated with the change of strength of the wing shock wave produced by the rear-fuselage modification (see Section 4.2).

7.2. Variation of Lift-curve Slope and Aerodynamic Centre with Mach Number.

The results have been analysed to obtain lift-curve slopes and aerodynamic-centre positions for the three configurations. These are plotted against Mach number in Figs. 41 and 42. To avoid the unstable region around zero lift at some Mach numbers (occurring only at values of $-C_z$ not attained in flight) the slopes have been obtained at $-C_z = 0.1$. The positions of the mean quarter-chord point and the mean half-chord point of the wing are shown on Fig. 42 for reference.

The standard deviations of the derived lift-curve slopes and aerodynamic-centre positions are estimated to be about 0.001 and 0.01 respectively.

The effect of the addition of the tail unit (Figs. 41a and 42a) is, as expected, a slight increase in lift-curve slope and an increase in the stability equivalent to a rearward shift of the aerodynamic centre by approximately 5% of the aerodynamic mean chord.

The effect of the rear-fuselage modification on lift-curve slope is seen (Fig. 41b) to be greatest at approximately $M = 0.96$. This can again be associated with the different strengths of the wing shock wave in the two cases. There is no difference in the position of the aerodynamic centre (Fig. 42b) except near $M = 1.04$ where it is 2% of the aerodynamic mean chord farther aft with the modified fuselage; the reliability of the results at this speed is doubtful owing to the possibility of reflection of the bow wave back on to the model (see Section 2.3).

The values of $-dC_z/d\alpha$ and $-dC_m/dC_z$ for the original planform (unkinked leading edge) from Ref. 3 are compared* in Figs. 41a and 42a with the results of the present tests. The aerodynamic-centre positions for the two planforms have been calculated for each wing at $M = 0.7$ by the method of Ref. 4. The estimated difference of 2.5% of the aerodynamic mean chord agrees with the experimental difference at $M = 0.7$ (Fig. 42a). In addition it will be seen that the rearward travel of the aerodynamic centre with increase of Mach number occurs at a Mach number approximately 0.02 higher in the present tests. It is not possible to say whether this arises from the change in the wing geometry or from wind-tunnel differences, the earlier results being obtained in a solid-wall working section while the present results were obtained in a slotted-wall working section.

7.3. Comparison of Aerodynamic-Centre Positions from Tunnel and Flight Tests.

The aerodynamic-centre positions obtained in the present tests are compared with results from flight tests in Fig. 43. The flight test results^{5,6} contain considerable scatter and for each Mach

* In order that the aerodynamic-centre positions from the earlier results (which were based on the geometric mean chord of the original wing) should be directly comparable with the present results they have been recalculated using the aerodynamic mean chord of the present wing as the reference length.

number have been analysed statistically to yield a mean value and a standard deviation of this mean value. Each vertical line plotted represents the mean value \pm its standard deviation. There is some doubt as to the true value of the Mach number in the range 0.90 to 0.975 due to possible inaccuracy in the position error correction; following a verbal suggestion from the Gloster Aircraft Company, Mach numbers within this range have been increased by 0.02.

In the aircraft flight tests, measurements were made of the loads on the tailplane; from these were derived moments about the aircraft centre of gravity and, hence, the aerodynamic centre of the wing, fuselage and fin *in the presence of* the tailplane. Thus the results should approximate to the tail-off condition and are compared in Fig. 42 with the tunnel results for the model with the tail unit off since this would then be the most directly comparable case tested. It is to be expected that the comparison may be affected by the differences between the two configurations in the Mach number range where the presence of the tail unit affects the wing shock position (*see* Fig. 40 and Section 7.1).

It will be seen that at Mach numbers below 0.85 the aerodynamic centre is 2.5% of the aerodynamic mean chord farther aft for the flight tests than for the tunnel tests. At Mach numbers around 0.95 there is more scatter in the flight test results and less satisfactory correlation between the two sets of results, the limits of the standard deviation band ranging from 6.5% aft of the tunnel tests at $M = 0.93$ to 4% forward at $M = 0.975$. At Mach numbers of 0.98 and 1.05 the results agreed to within about 1%.

8. Conclusions.

Force measurements and flow observations on a 1/72 scale model of the *Javelin* aircraft show directional instability near sonic speed, as observed in flight due to shock-induced separation on the fin; this appears to have been caused by the wing trailing-edge shock wave strengthened by the flow fields of the fin and rear fuselage.

The shock strength was reduced and the separation delayed to higher wing incidences by a small change of shape of the rear fuselage. In this condition the variation of yawing moment with angle of sideslip was stable. Vortex generators also improved the flow over the fin. Modification to the shape and thickness distribution of the lower half of the fin and the addition of a 'bullet' in the fin-tailplane junction had no beneficial effects on the stability nor on the flow over the fin.

Flight observations and the tunnel results for the basic aircraft and the aircraft with the modified rear fuselage were in good qualitative agreement.

The significant effect that a small distortion of the fuselage shape at the tail, such as might be made to accommodate a supporting sting, can have on directional stability is of general importance from the point of view of wind-tunnel testing techniques.

Tests of longitudinal stability show that the curves of pitching moment against normal force have stable slopes throughout the incidence and Mach number ranges covered except near zero lift at isolated Mach numbers. The stability decreases at high incidence at $M = 0.7$ and at moderate incidence around $M = 0.93$.

Comparison of aerodynamic-centre positions from the tunnel tests and from aircraft flight tests shows reasonable qualitative agreement in general; differences of the order of 2.5% of the aerodynamic mean chord occur at Mach numbers below 0.85, 1% at Mach numbers of 0.98 and 1.05, and larger differences at Mach numbers between 0.85 and 0.98.

LIST OF SYMBOLS

b	Wing span
\bar{c}	Aerodynamic mean chord
C_m	Pitching moment/ $\frac{1}{2}\rho V^2 S \bar{c}$ (<i>see</i> Fig. 1 for sign and Table 1 for moment centre)
C_n	Yawing moment/ $\frac{1}{2}\rho V^2 S b$ (<i>see</i> Fig. 1 for sign and Table 1 for moment centre)
C_Y	Side force/ $\frac{1}{2}\rho V^2 S$ (<i>see</i> Fig. 1 for sign)
$-C_z$	Normal force/ $\frac{1}{2}\rho V^2 S$ (<i>see</i> Fig. 1 for sign)
M	Mach number
R	Reynolds number (based on \bar{c})
S	Gross wing area
V	Free-stream velocity
v	Component of free-stream velocity in direction of negative y -axis (<i>see</i> Fig. 1)
w	Component of free-stream velocity in direction of negative z -axis (<i>see</i> Fig. 1)
α	Angle of incidence = $\arctan w/(V^2 - v^2 - w^2)^{1/2}$ (<i>see</i> Fig. 1)
β	Angle of sideslip = $\arcsin v/(V^2 - v^2)^{1/2}$ (<i>see</i> Fig. 1)
ρ	Density of free stream

REFERENCES

<i>No.</i>	<i>Author(s)</i>	<i>Title, etc.</i>
1	E. P. Sutton	The development of slotted working-section liners for transonic operation of the R.A.E. Bedford, 3-ft Wind Tunnel. A.R.C. R. & M. 3085. March, 1955.
2	H. H. Pearcey	Some effects of shock-induced separation of turbulent boundary-layers in transonic flow past aerofoils. Symposium 'Boundary layer effects in aerodynamics'. H.M.S.O., London, 1955.
3	A. B. Haines and D. S. Capps ..	High speed tunnel test on a twin-engined fighter of delta planform (Gloster F4/48). R.A.E. Report Aero. 2359. March, 1950.
4	D. Kuchemann	A simple method for calculating the span and chordwise loadings on thin swept wings. R.A.E. Report Aero. 2392. A.R.C. 13 758. August, 1950.
5	—	Interim report on tail load measurements on WT 830. Gloster Aircraft Company. G.A.5 Flight Aerodynamics, Book 4, Part 6. September, 1955.
6	—	Javelin WT 830. Transonic tail load measurements. Gloster Aircraft Company. G.A.5 Flight Aerodynamics, Book 4, Part 8. May, 1956.

TABLE 1—*continued**Tailplane*

Gross area	3·187 sq. in.
Span	2·833 in.
Standard mean chord	1·125 in.
Aerodynamic mean chord	1·293 in.
Chord at centre line	1·875 in.
Tip chord	0·375 in.
Taper ratio	0·200
Aspect ratio	2·51
Sweepback of leading edge	50·0°
Section	RAE 101 (Symmetrical, 9% <i>t/c</i> , T.E. angle 9·2°)
Dihedral	0
Setting relative to wing	0
Height above wing plane	1·750 in.
Distance of mean quarter-chord point behind moment centre	3·535 in.

Fin

Exposed area	3·067 sq. in.
Height from centre line	1·750 in.
Root chord	2·472 in.
Tip chord	1·833 in.
Aspect ratio of exposed area	0·62
Sweepback of leading edge	50·2°
Sweepback of trailing edge	36·4°
Section	RAE 101 (Symmetrical, 9% <i>t/c</i> , T.E. angle 9·2°)
Distance of mean quarter-chord point behind moment centre	2·289 in.
Distance of centre of area behind moment centre	2·831 in.

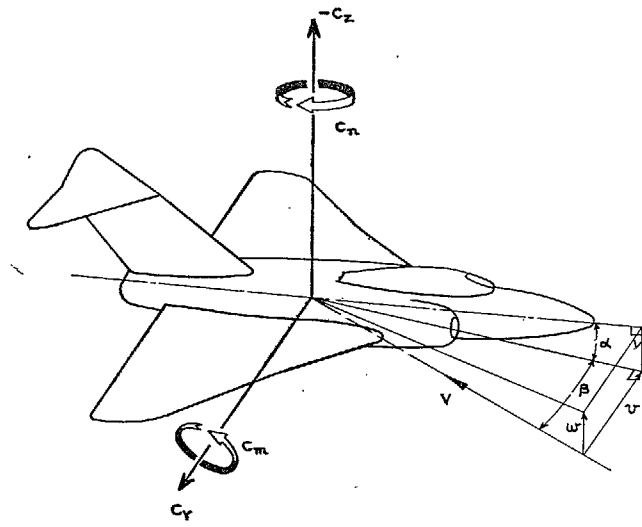
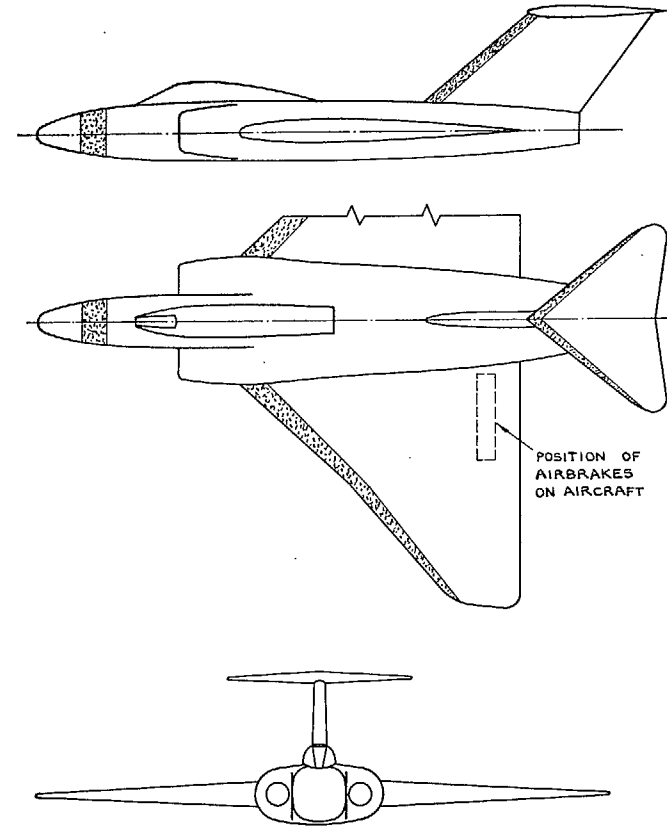



FIG. 1. Definitions of forces, moments and angles.



 EXTENT OF CARBORUNDUM BANDS FOR BOUNDARY-LAYER TRANSITION FIXING

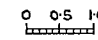
 0.05 INCH
 MODEL SCALE

FIG. 2. Layout of the wind-tunnel model.

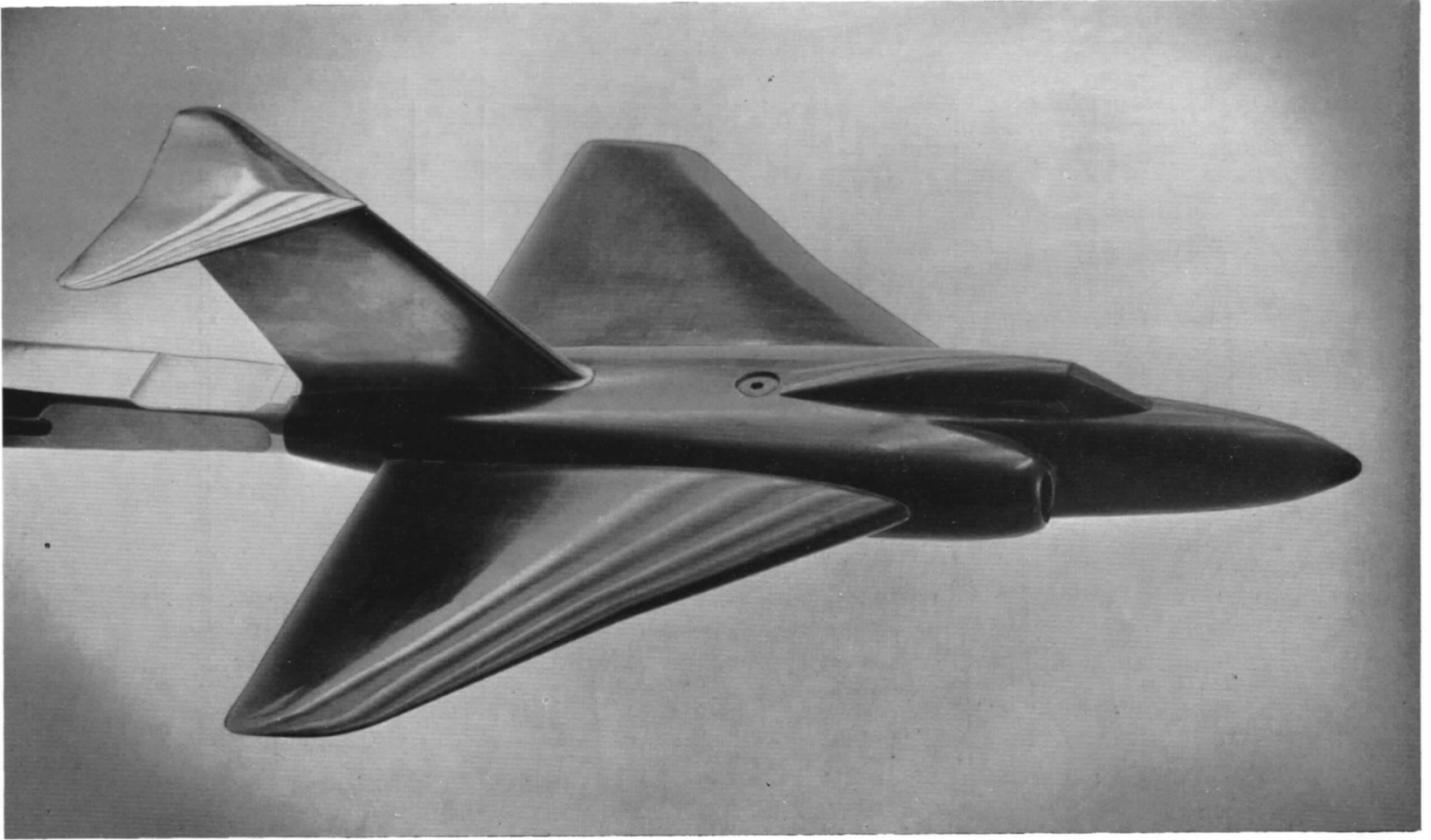


FIG. 3. Model on the sting before attachment of the strain gauges.

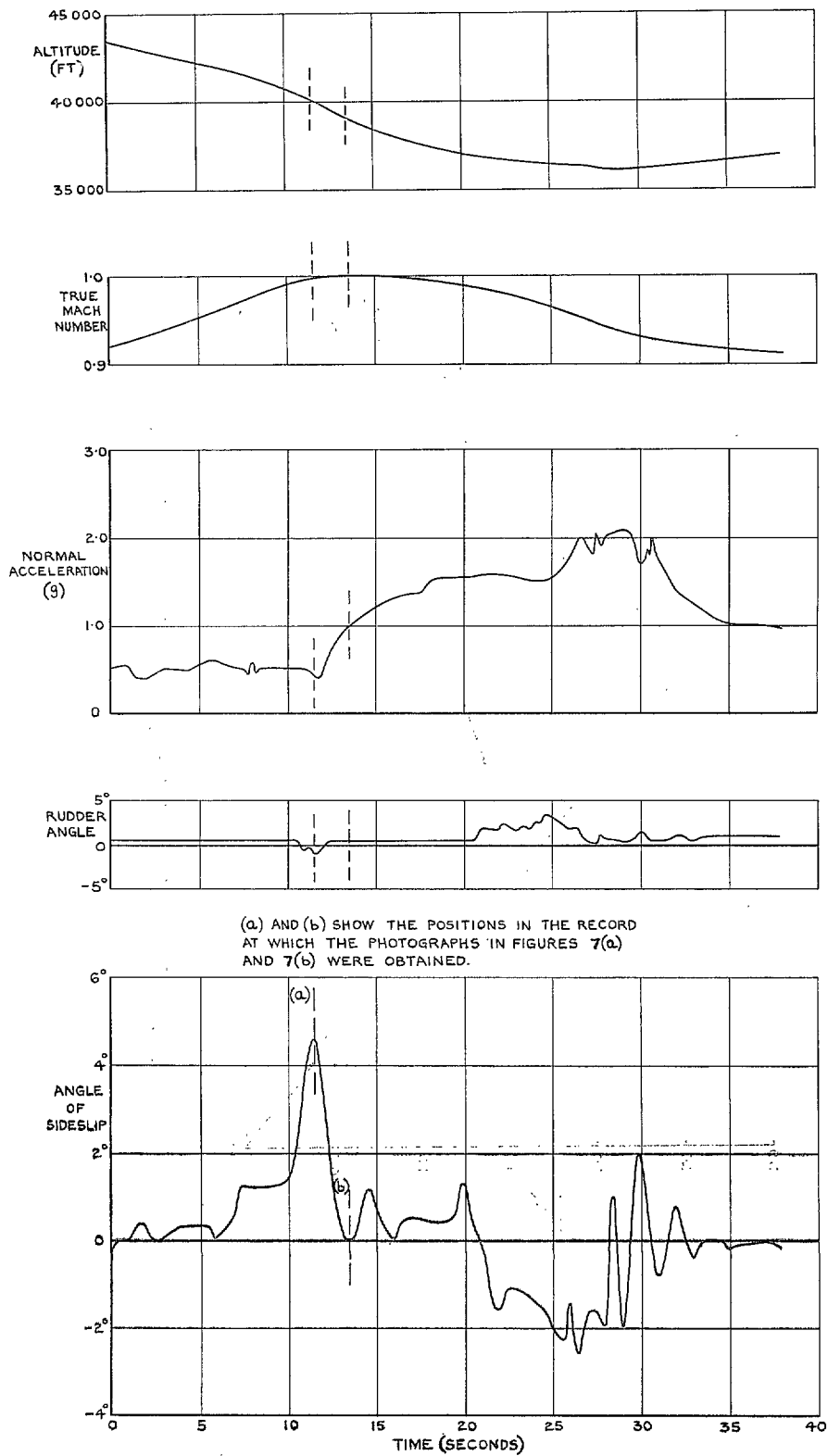
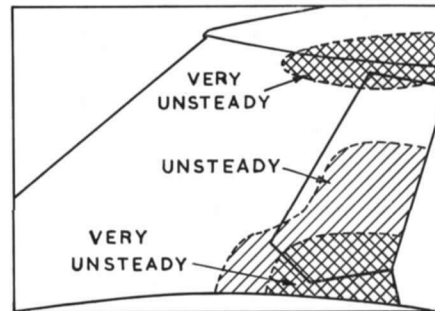
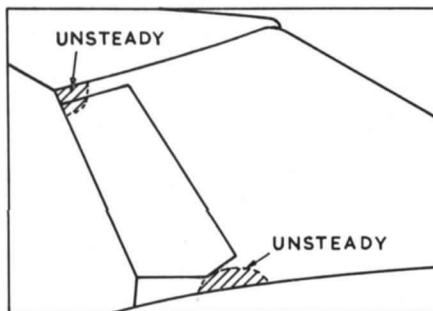
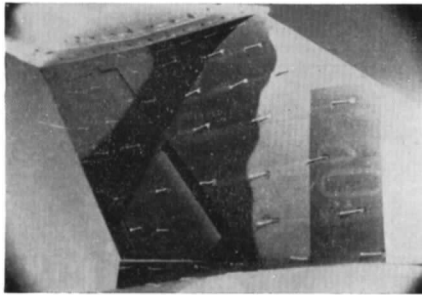


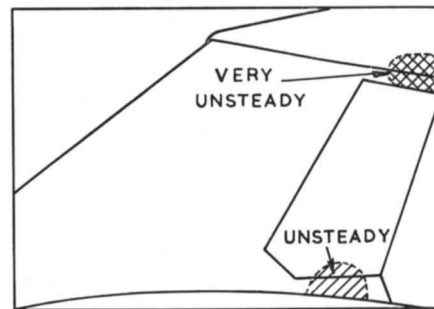
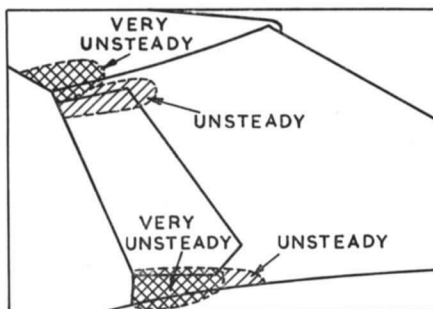
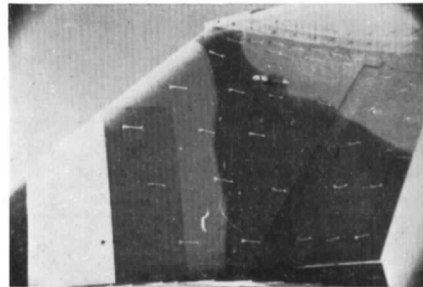
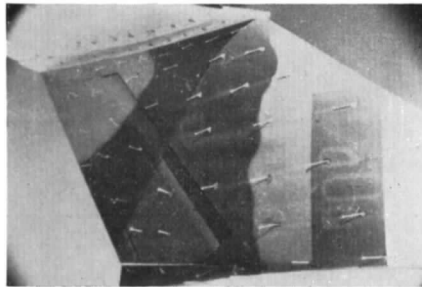
FIG. 6. Typical record of a transonic dive.

SUCTION SURFACE OF FIN

PRESSURE SURFACE OF FIN



(a) $M = 0.99 - 1.00$ SIDESLIP = 4.6° RUDDER DEFLECTION -0.8°



(b) $M = 1.00$ SIDESLIP = 0 RUDDER DEFLECTION $+0.5^\circ$

FIG. 7a and b. Typical tuft photograph obtained during a transonic dive.

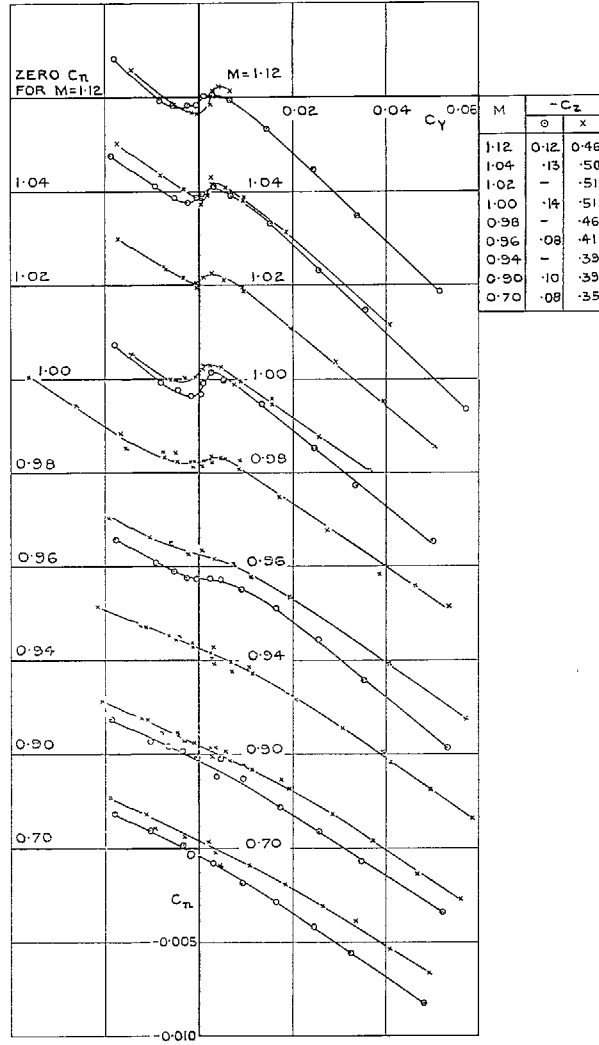


FIG. 8. Variation of C_n with C_Y for the basic configuration with the tail unit on.

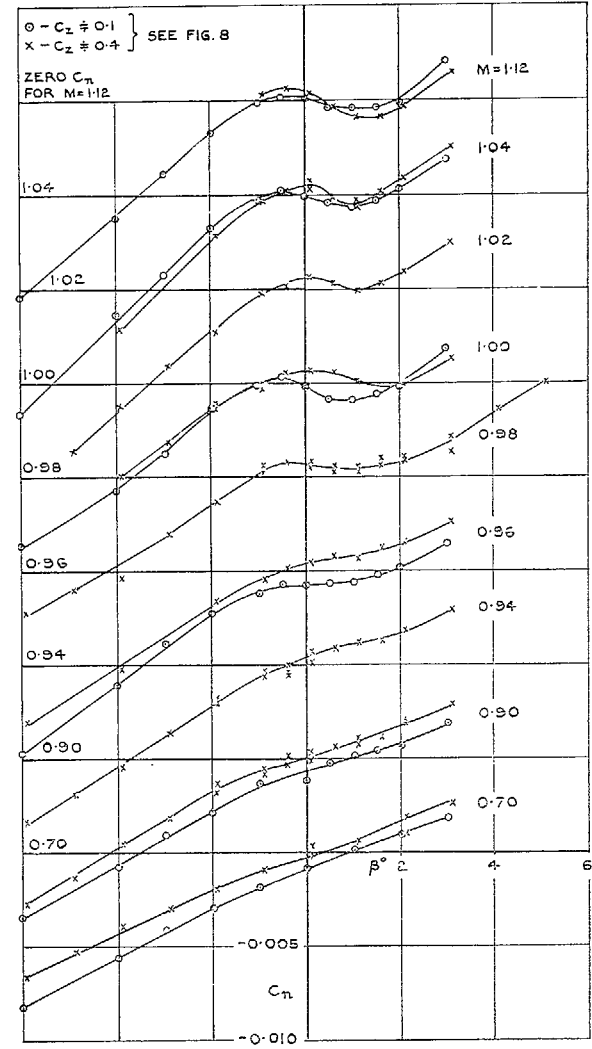


FIG. 9. Variation of C_n with β for the basic configuration with the tail unit on.

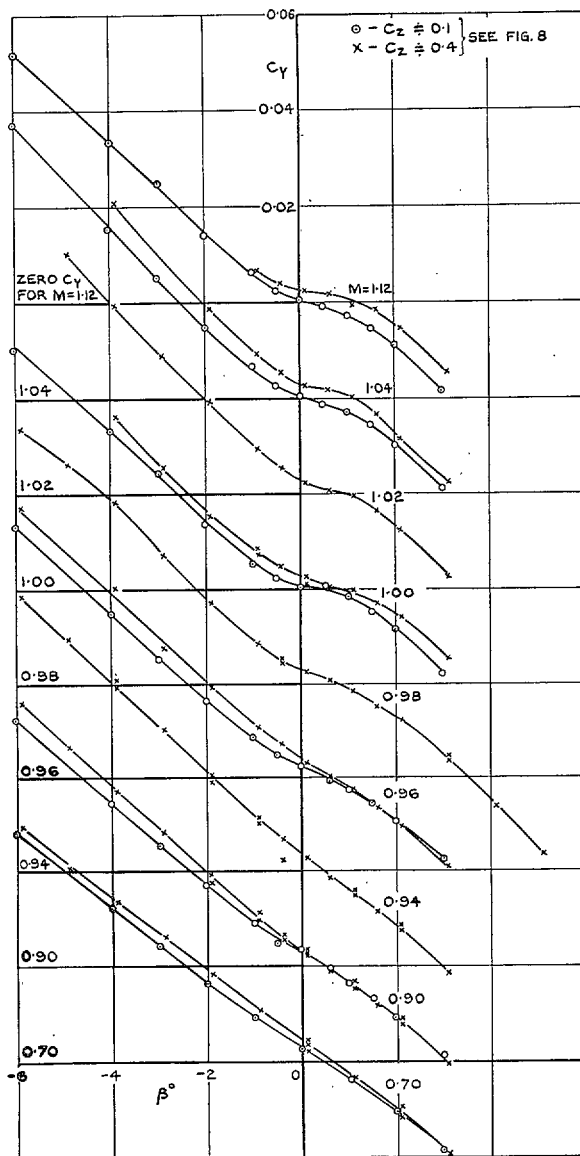


FIG. 10. Variation of C_Y with β for the basic configuration with the tail unit on.

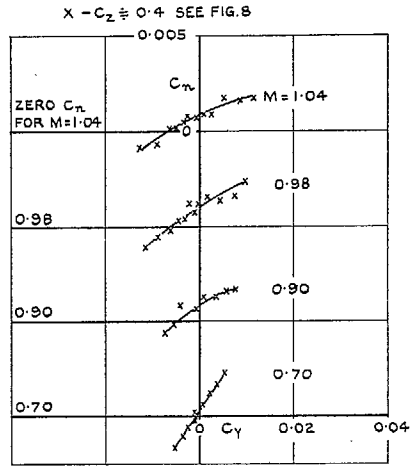


FIG. 11. Variation of C_n with C_y for the basic configuration with the tail unit off.

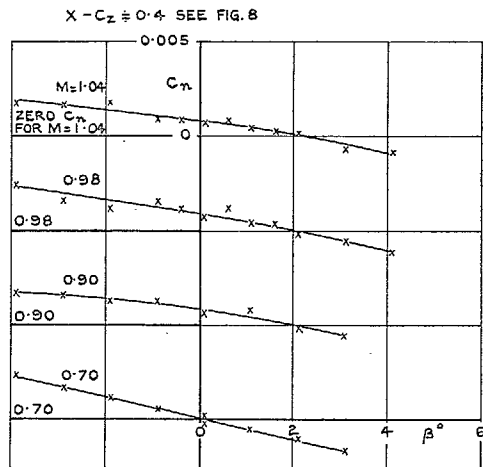


FIG. 12. Variation of C_n with β for the basic configuration with the tail unit off.

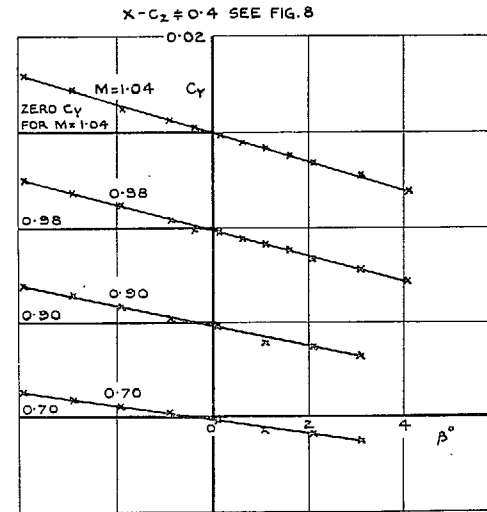


FIG. 13. Variation of C_y with β for the basic configuration with the tail unit off.

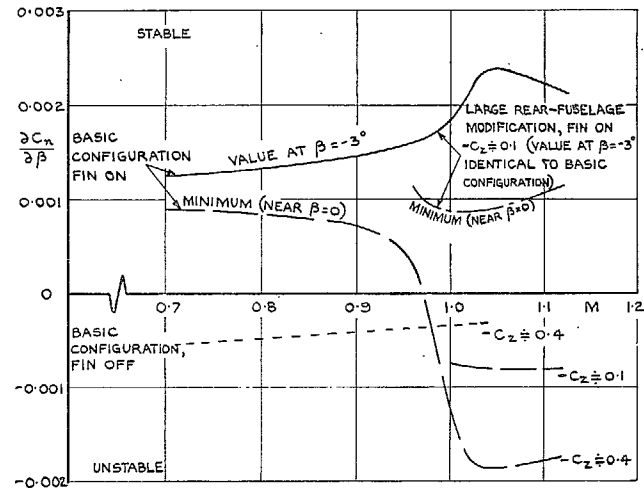
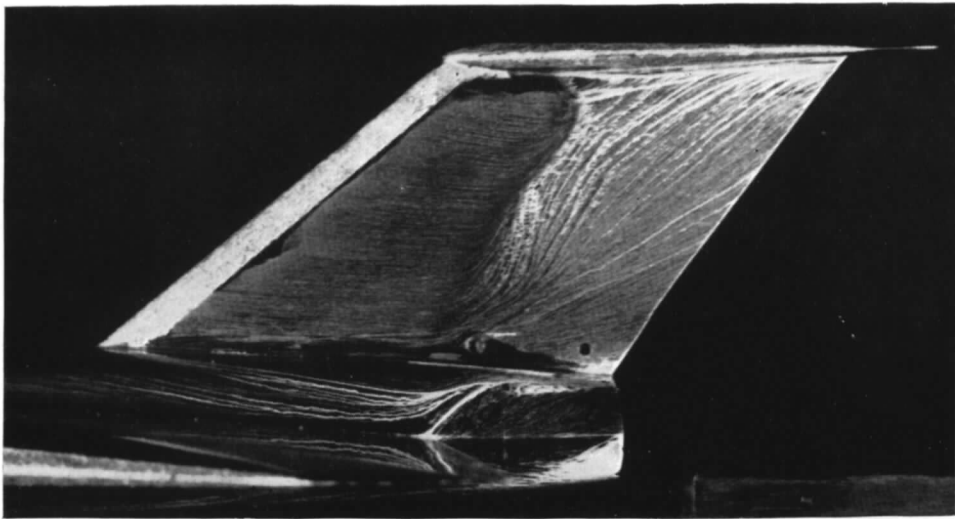


FIG. 14. Variation of $\frac{\partial C_n}{\partial \beta}$ with Mach number.

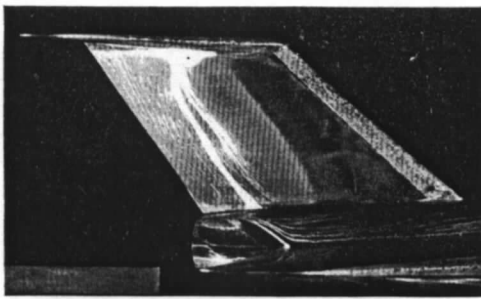


STARBOARD

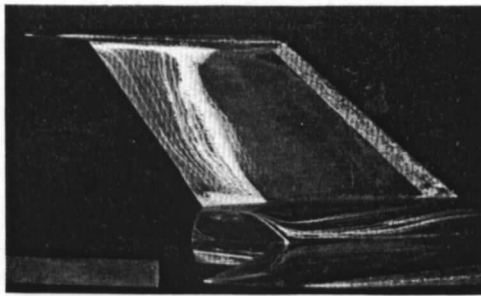
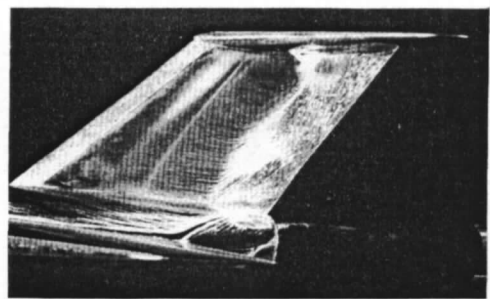


PORT

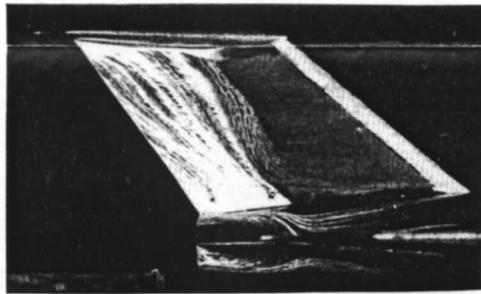
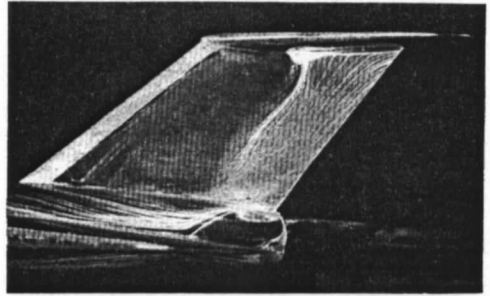
FIG. 15. Oil-flow patterns on the fin at $M = 1.00$, $-C_z = 0.14$, $\beta = 0$.



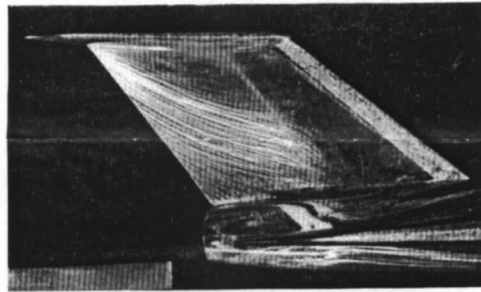
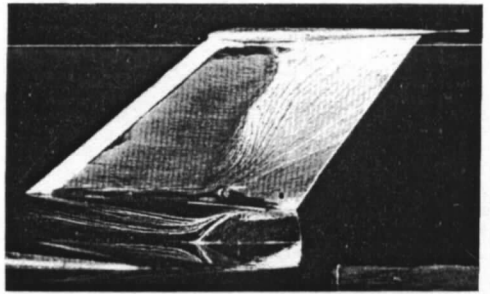
e
 $M = 1.12$
 $-C_z = 0.16$



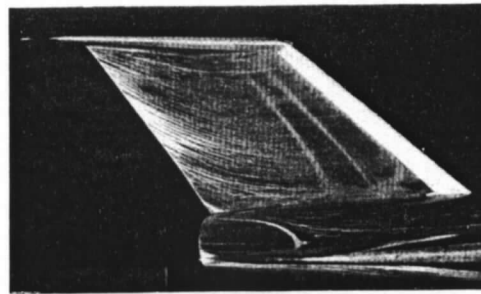
d
 $M = 1.04$
 $-C_z = 0.18$



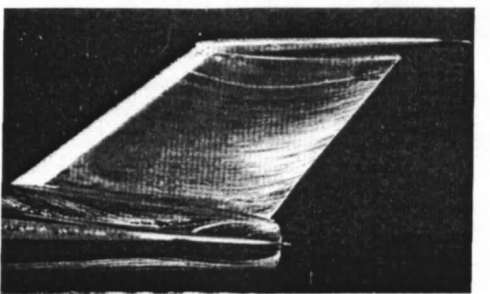
c
 $M = 1.00$
 $-C_z = 0.14$



b
 $M = 0.96$
 $-C_z = 0.11$



a
 $M = 0.90$
 $-C_z = 0.40$



STARBOARD

PORT

FIG. 16. Development of the separation from the fin with increase in Mach number; $\beta = 0$.

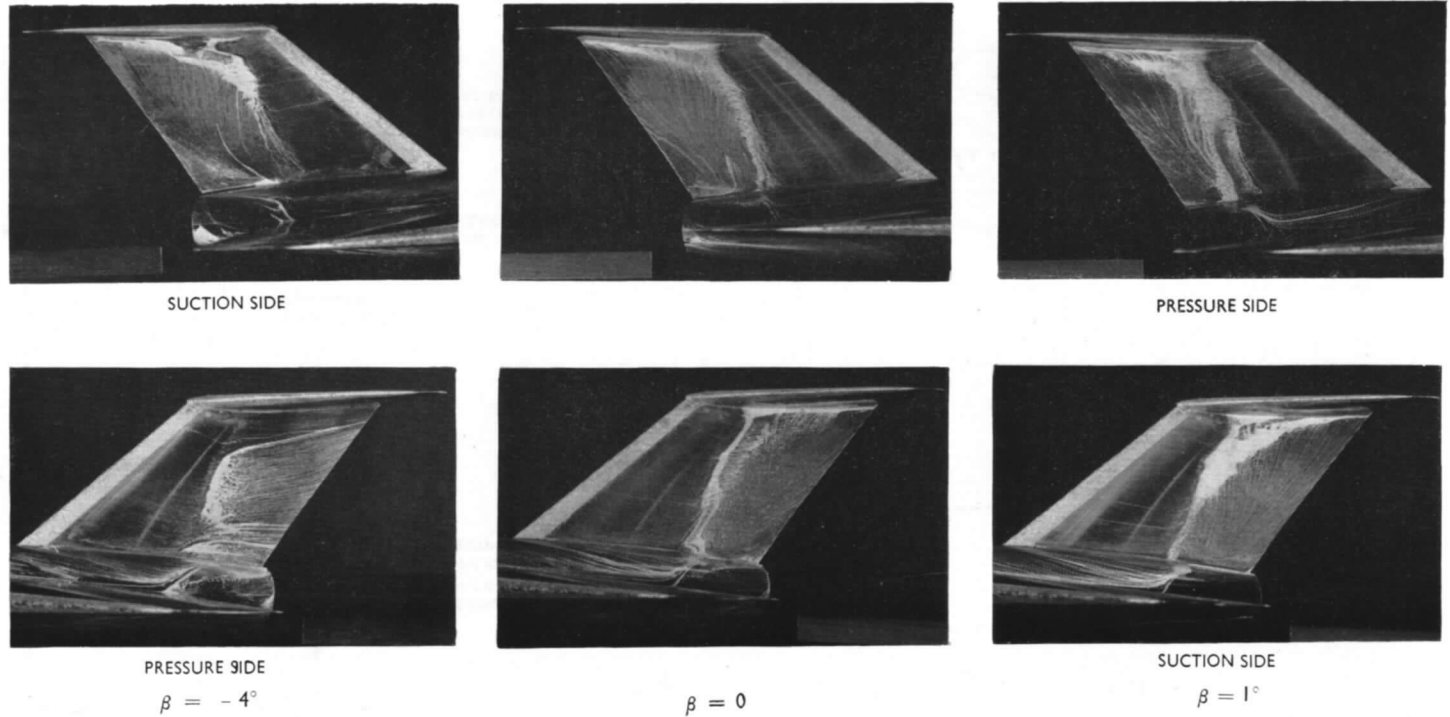


FIG. 17. Variation of the flow pattern on the fin with sideslip at $M = 1.00$, $-C_z = 0.51$.

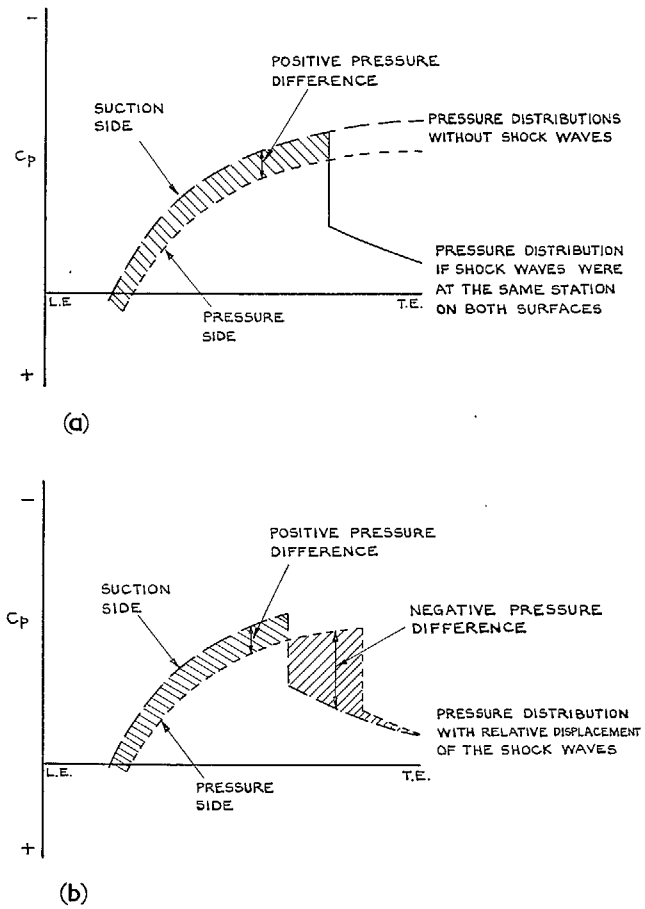


FIG. 18. Possible types of pressure distribution on the fin at small angles of sideslip at near-sonic speeds.

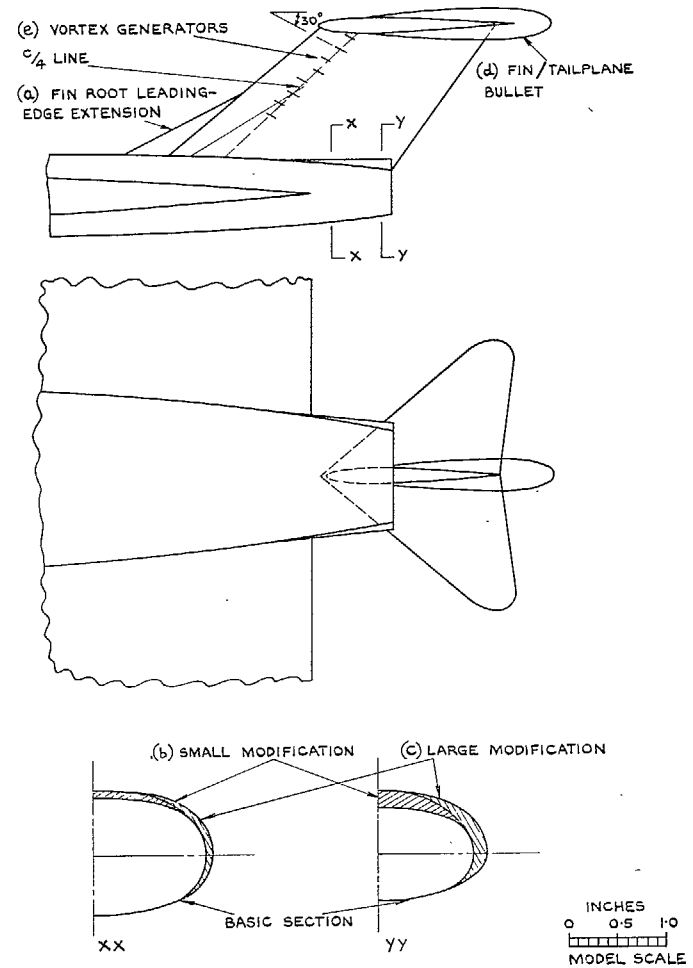


FIG. 19. Modifications of the basic configuration.

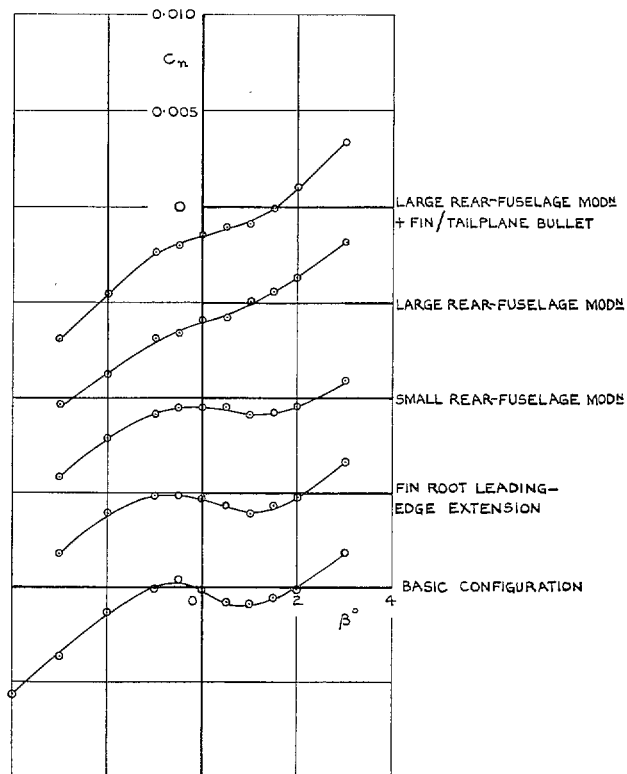


FIG. 20. Effect of modifications on the variation of C_n with β at $M = 1.00$. Tail unit on, $-C_z \doteq 0.14$.

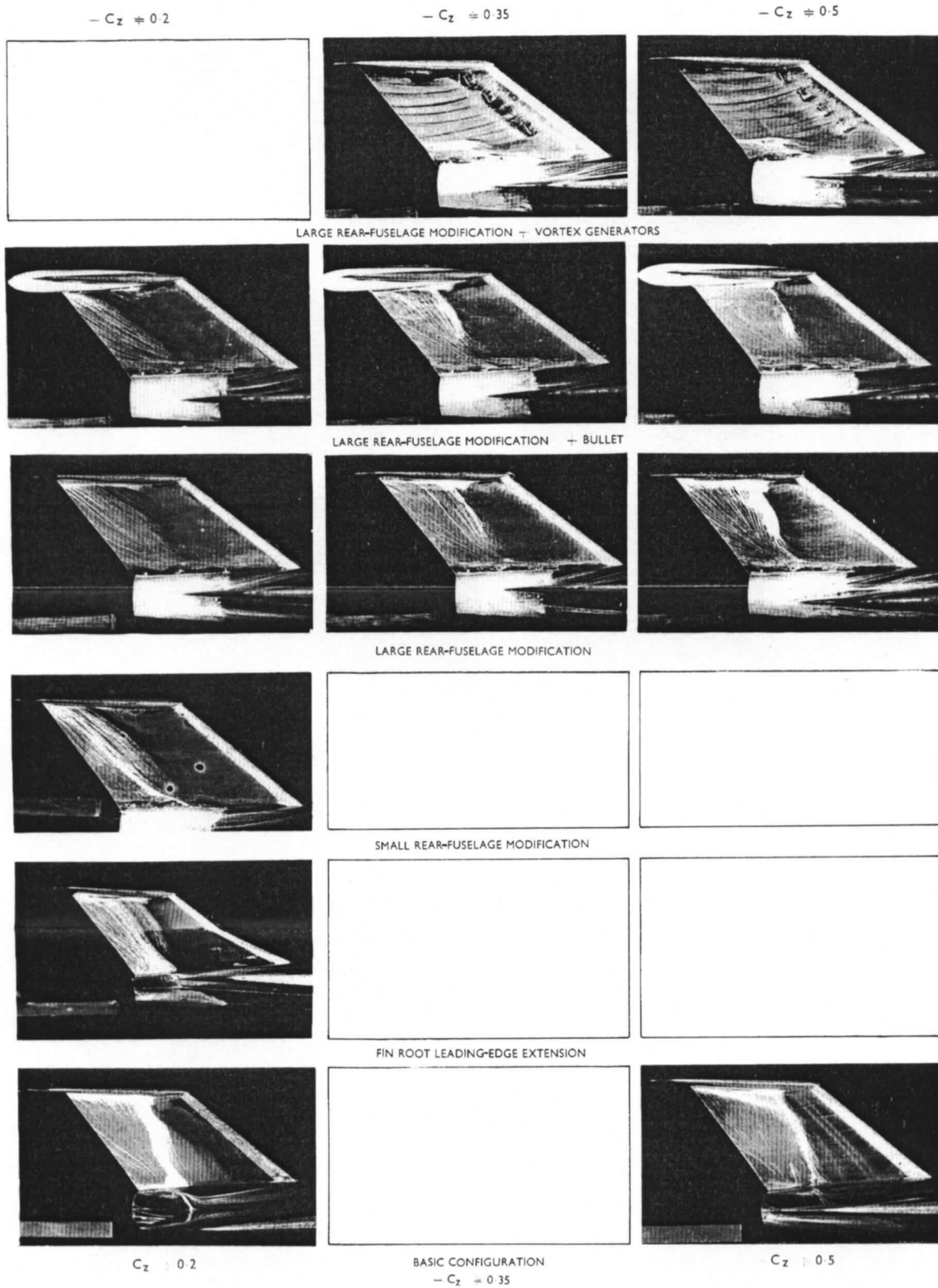


FIG. 21. Effect of modifications on the oil-flow patterns at $M = 1.00$, $\beta = 0$.

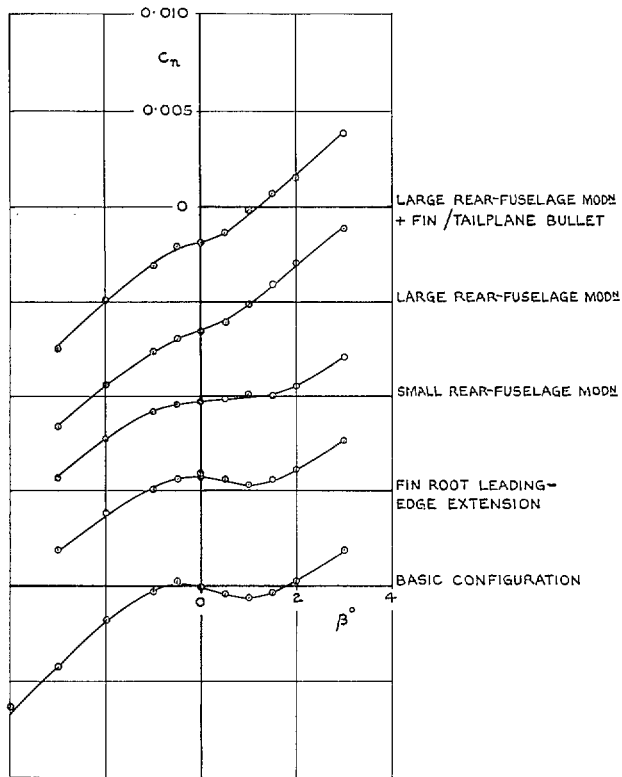
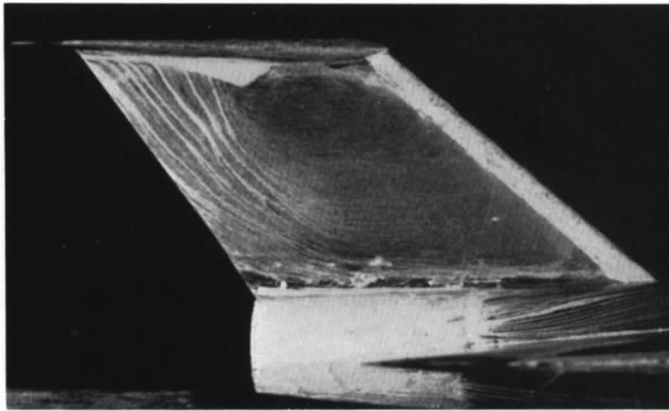
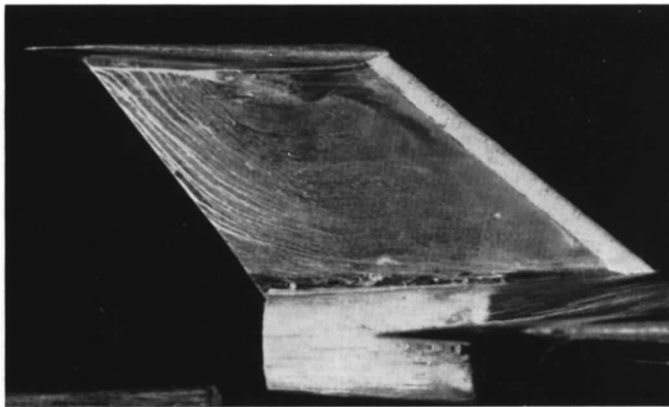


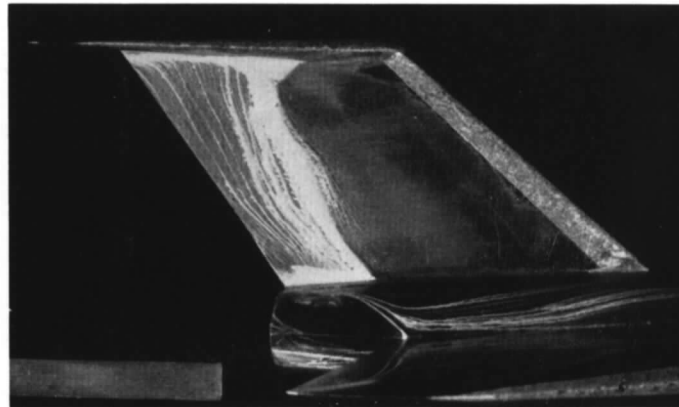
FIG. 22. Effect of modifications on the variation of C_n with β at $M = 1.04$. Tail unit on, $-C_z \doteq 0.13$.



Large rear fuselage modification $-C_z = 0.33$.



Large rear fuselage modification $-C_z = 0.18$.



Basic configuration $-C_z = 0.18$.

FIG. 23. Effect of rear-fuselage modification on the oil-flow pattern at $M = 1.04$, $\beta = 0$.

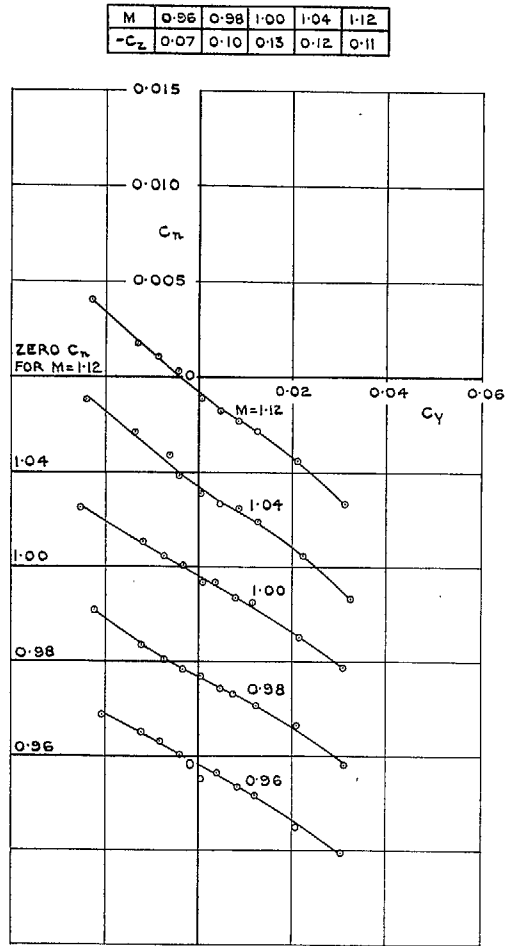


FIG. 24. Variation of C_n with C_Y with the large rear-fuselage modification and with the tail unit on.

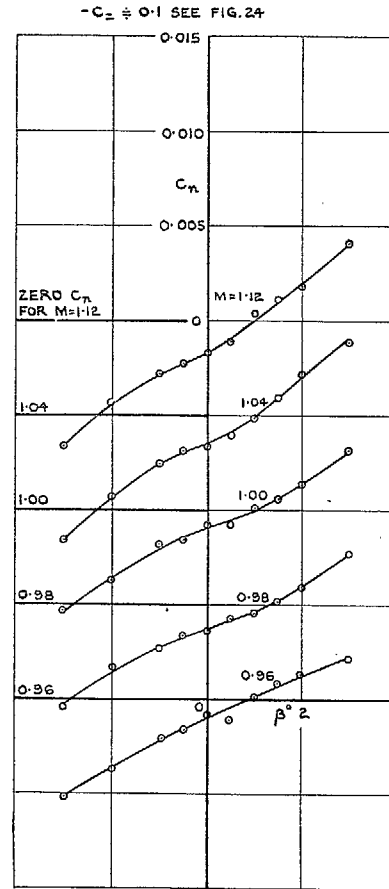


FIG. 25. Variation of C_n with β with the large rear-fuselage modification and with the tail unit on.

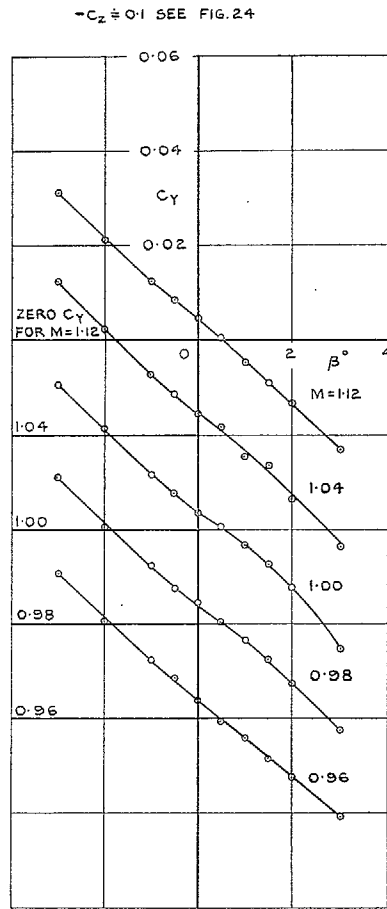


FIG. 26. Variation of C_Y with β with the large rear-fuselage modification and with the tail unit on.

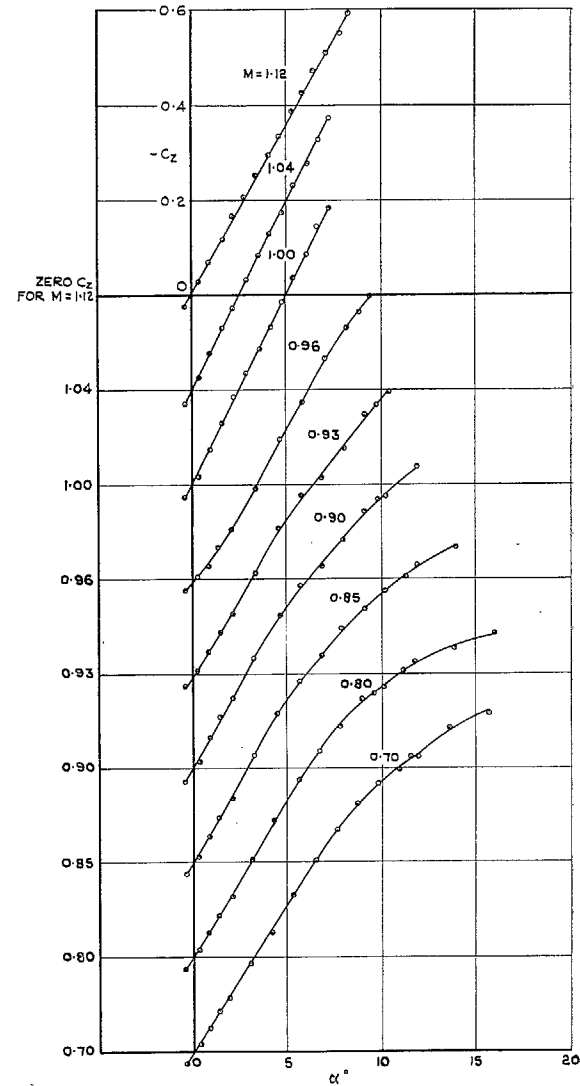


FIG. 27. Variation of $-C_z$ with α for the basic aircraft with the tail unit off.

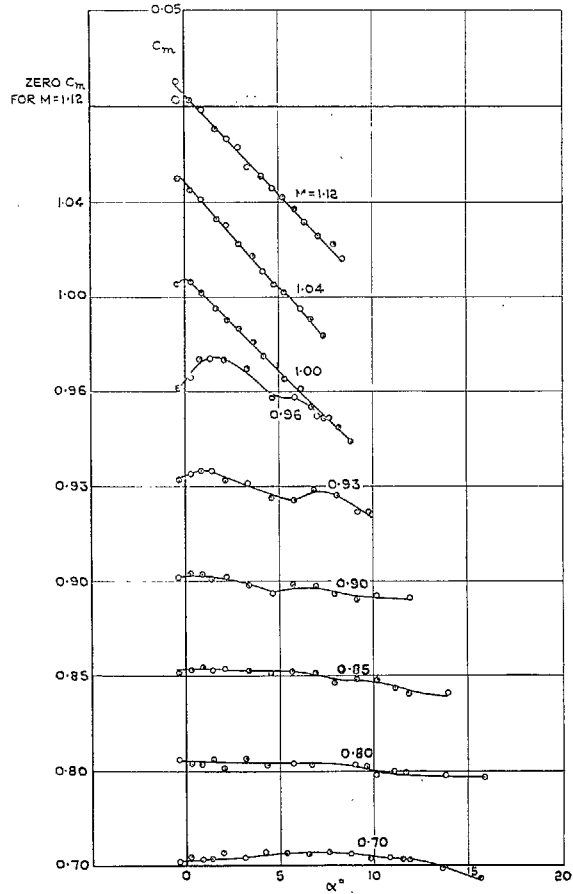


FIG. 28. Variation of C_m with α for the basic aircraft with the tail unit off.

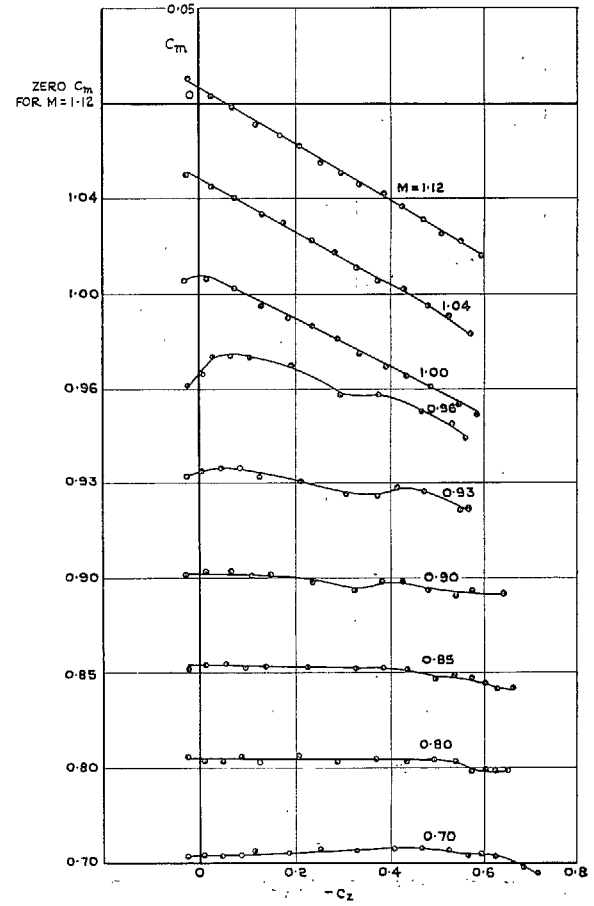


FIG. 29. Variation of C_m with $-C_z$ for the basic aircraft with the tail unit off.

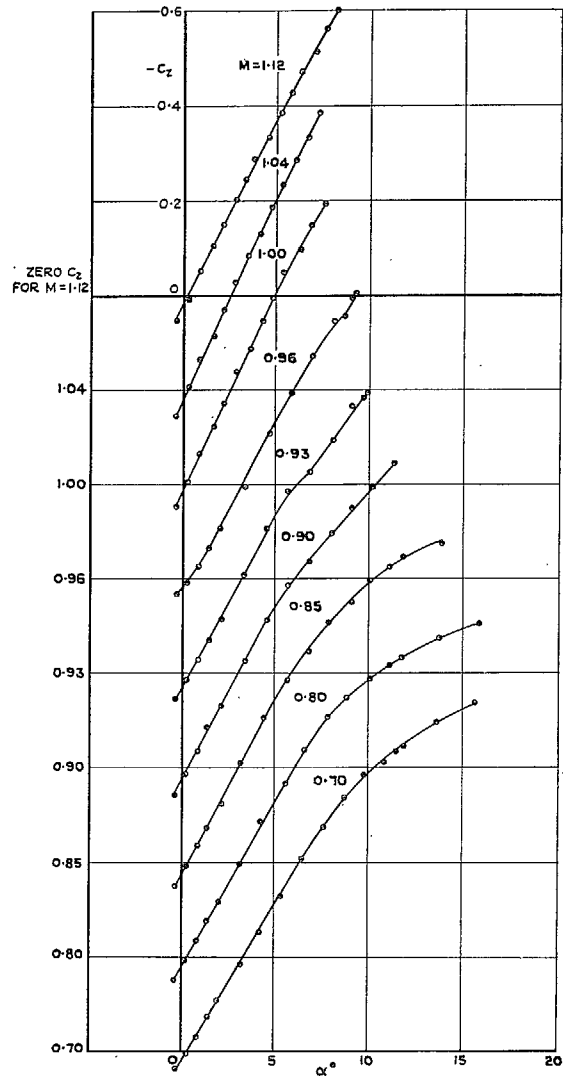


FIG. 30. Variation of $-C_z$ with α for the basic aircraft with the tail unit on.

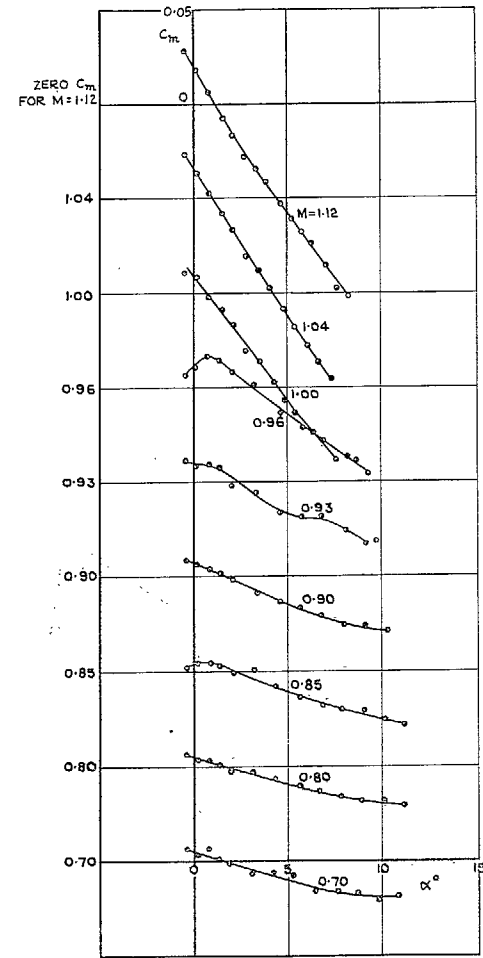


FIG. 31. Variation of C_m with α for the basic aircraft with the tail unit on.

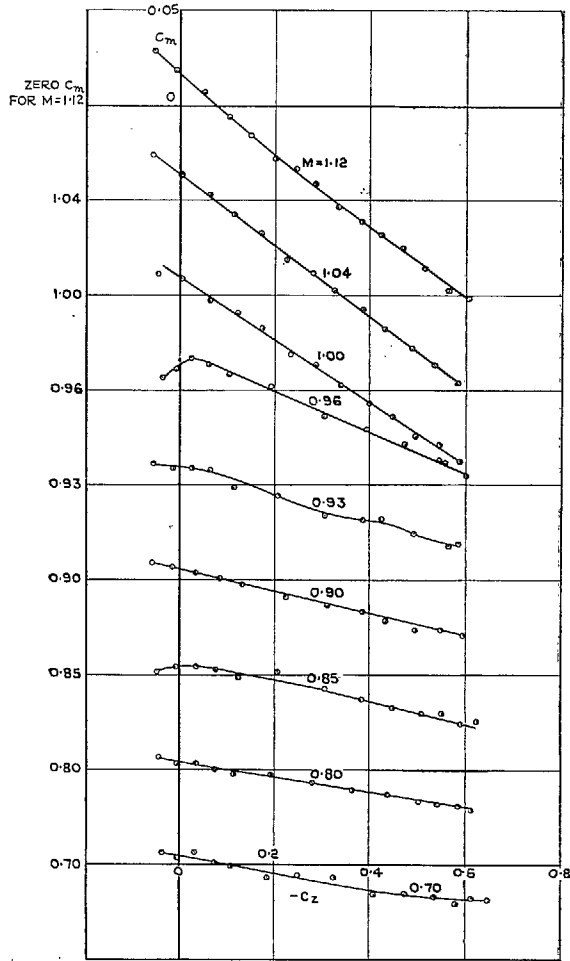


FIG. 32. Variation of C_m with $-C_z$ for the basic aircraft with the tail unit on.

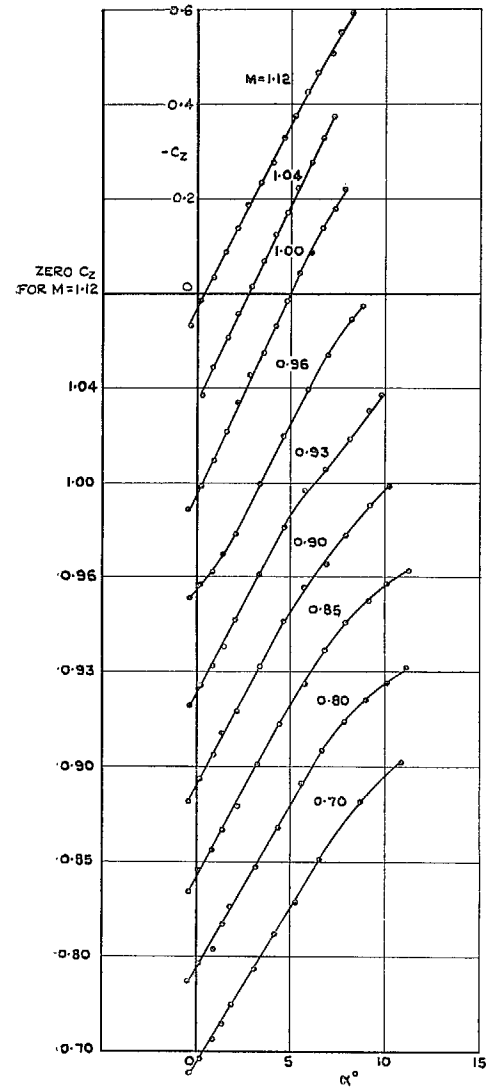


FIG. 33. Variation of $-C_z$ with α for the aircraft with the large rear-fuselage modification and with the tail unit on.

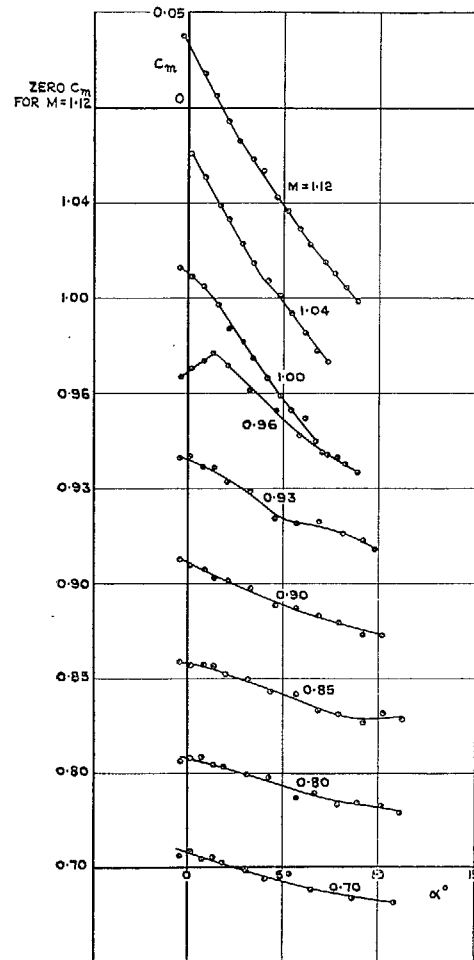


FIG. 34. Variation of C_m with α for the aircraft with the large rear-fuselage modification and with the tail unit on.

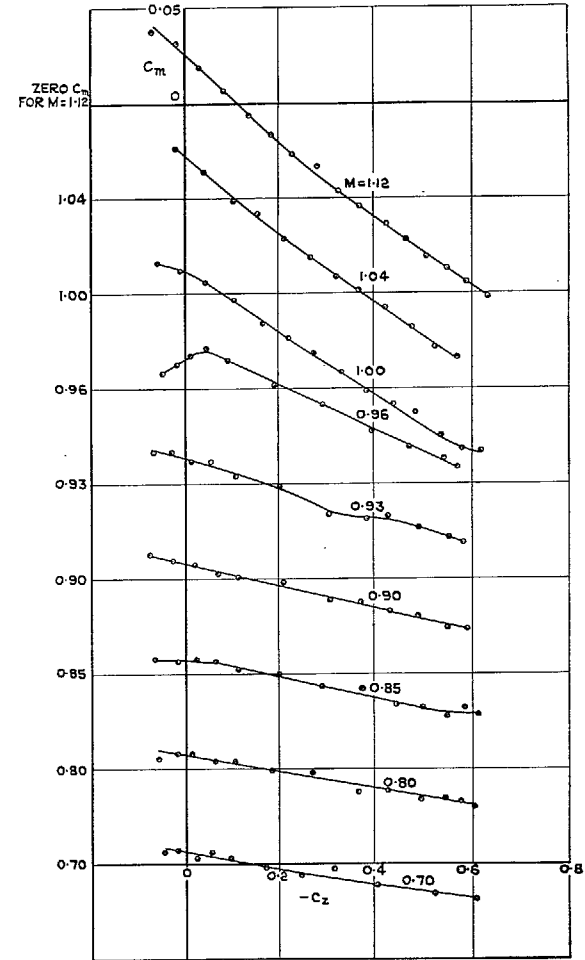


FIG. 35. Variation of C_m with $-C_z$ for the aircraft with the large rear-fuselage modification and with the tail unit on.

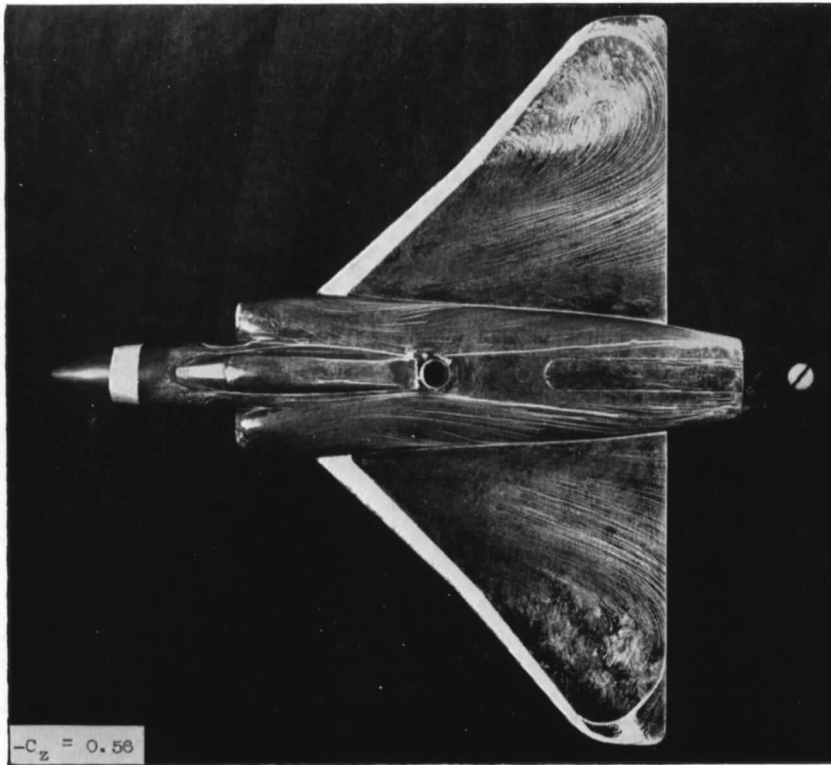
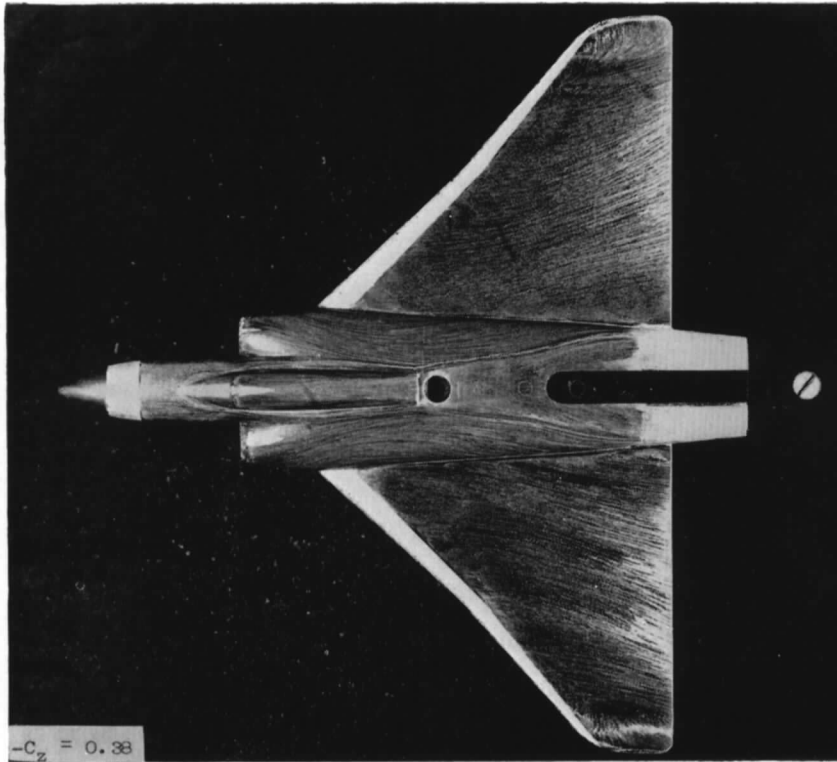


FIG. 36. Oil-flow patterns on wing at $M = 0.70$.

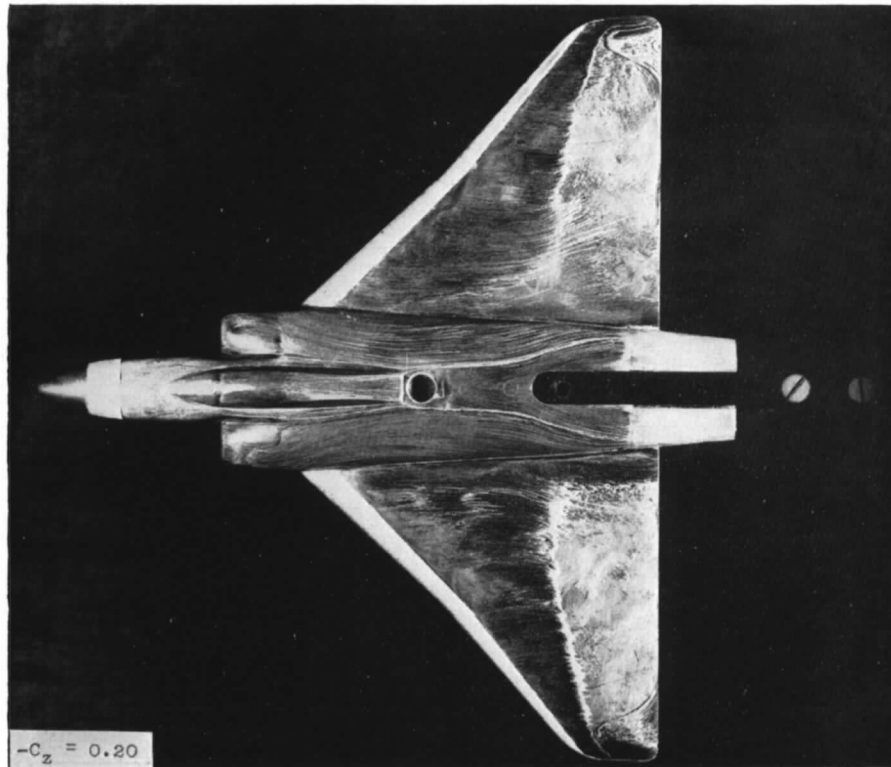
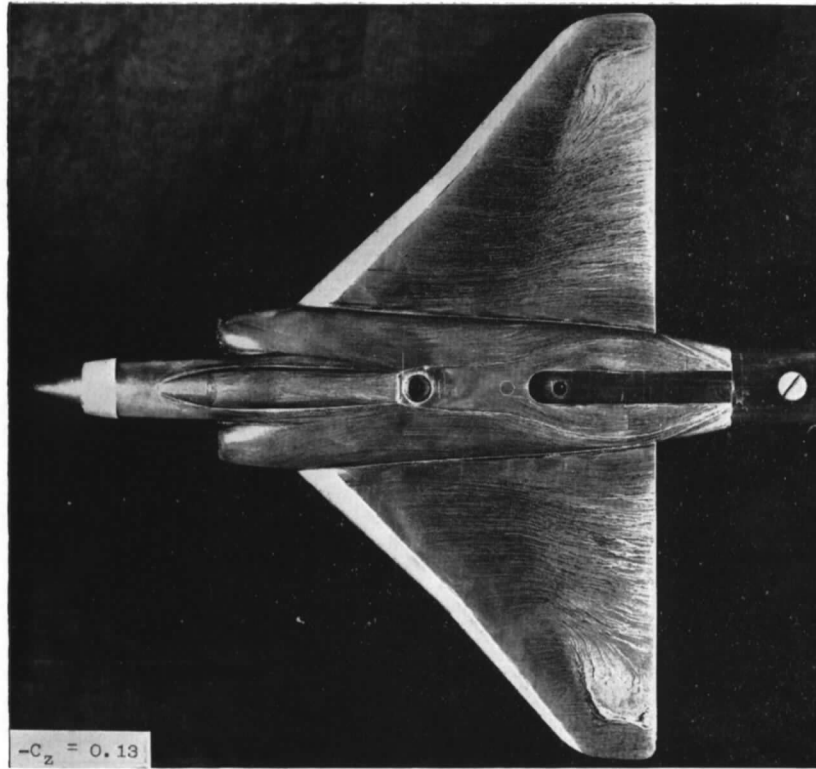


FIG. 37. Oil-flow patterns on wing at $M = 0.90$.

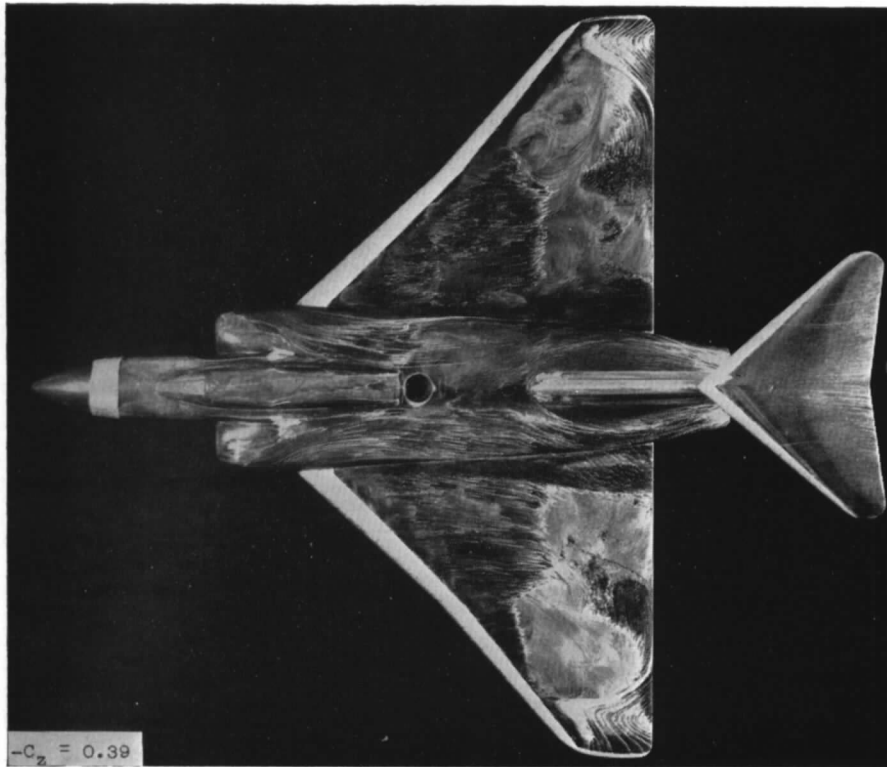
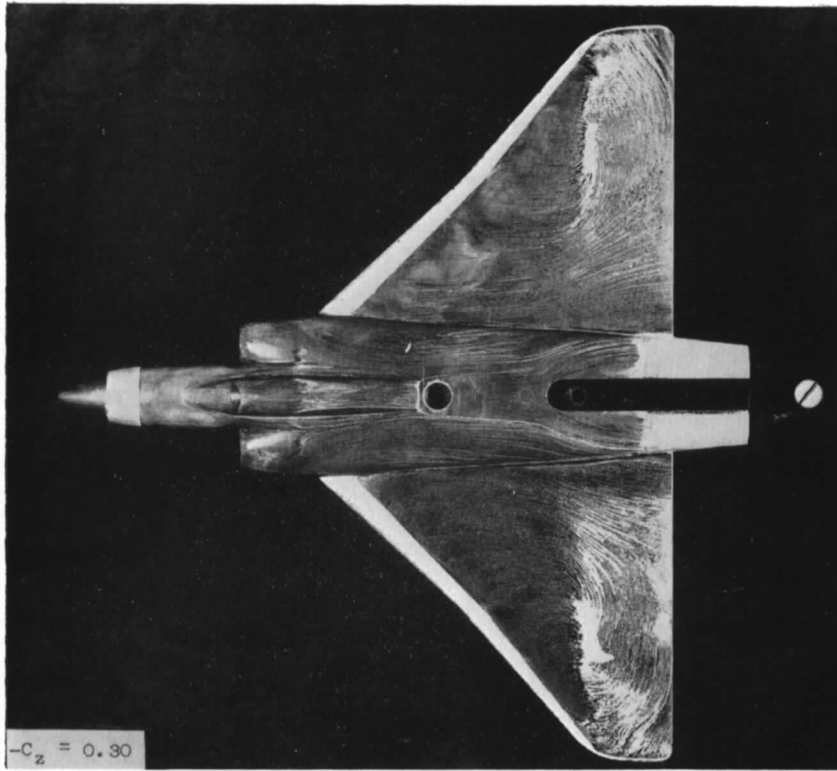


FIG. 37 (continued). Oil-flow patterns on wing at $M = 0.90$.

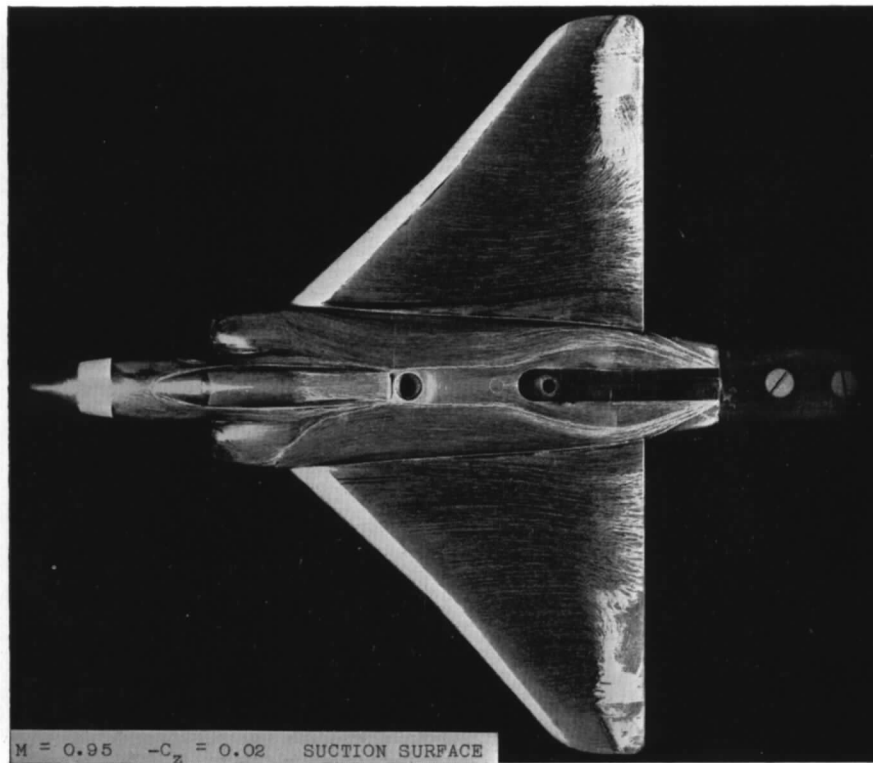
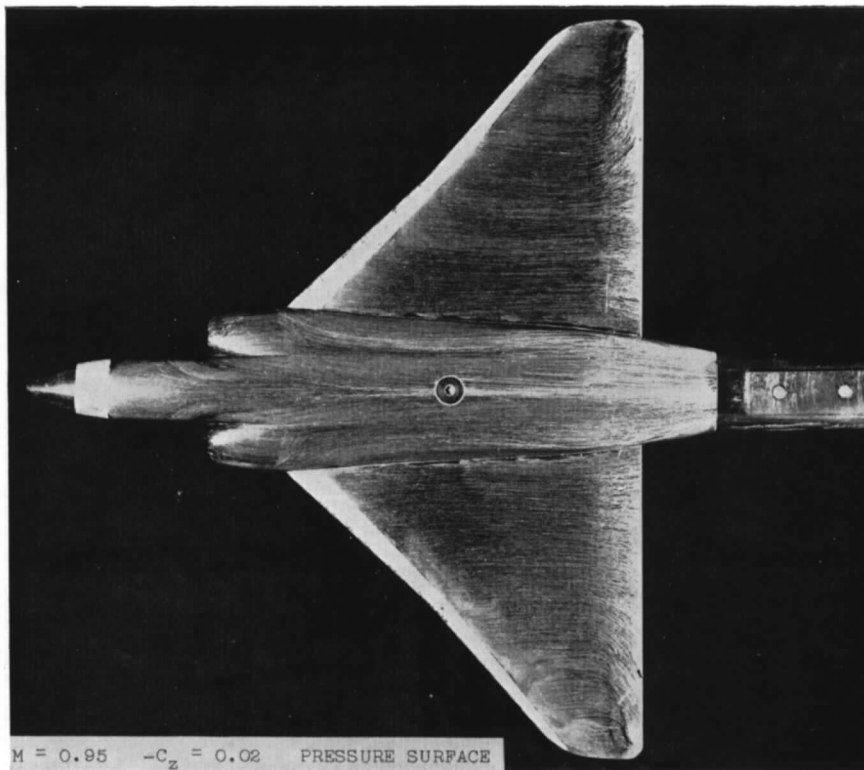


FIG. 38. Oil-flow patterns on wing at $M \doteq 0.96$.

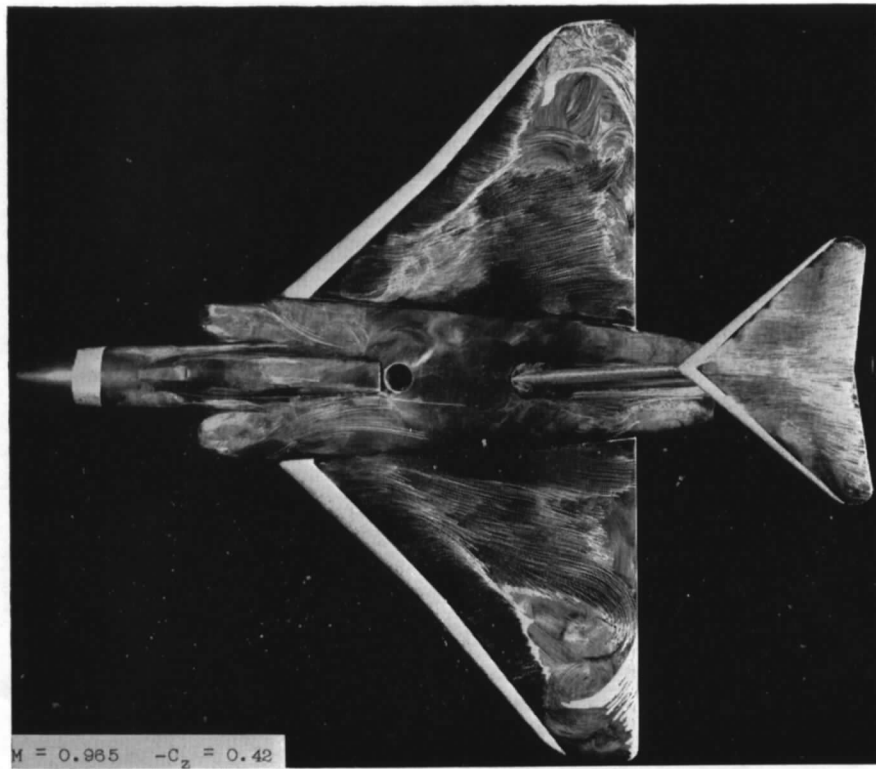
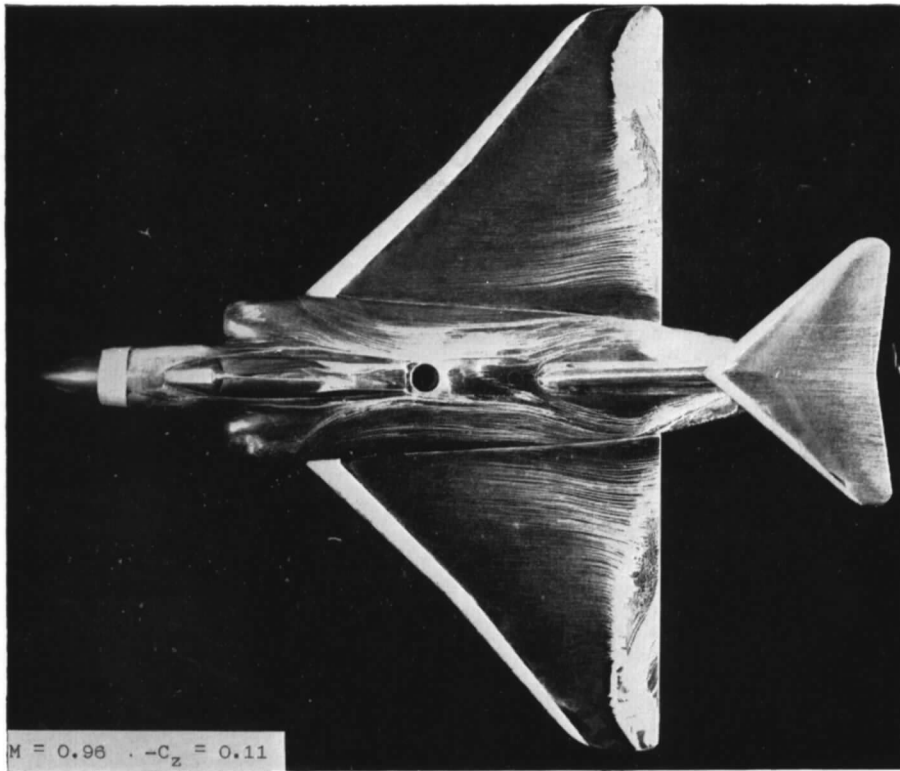


FIG. 38 (continued). Oil-flow patterns on wing at $M \doteq 0.96$.

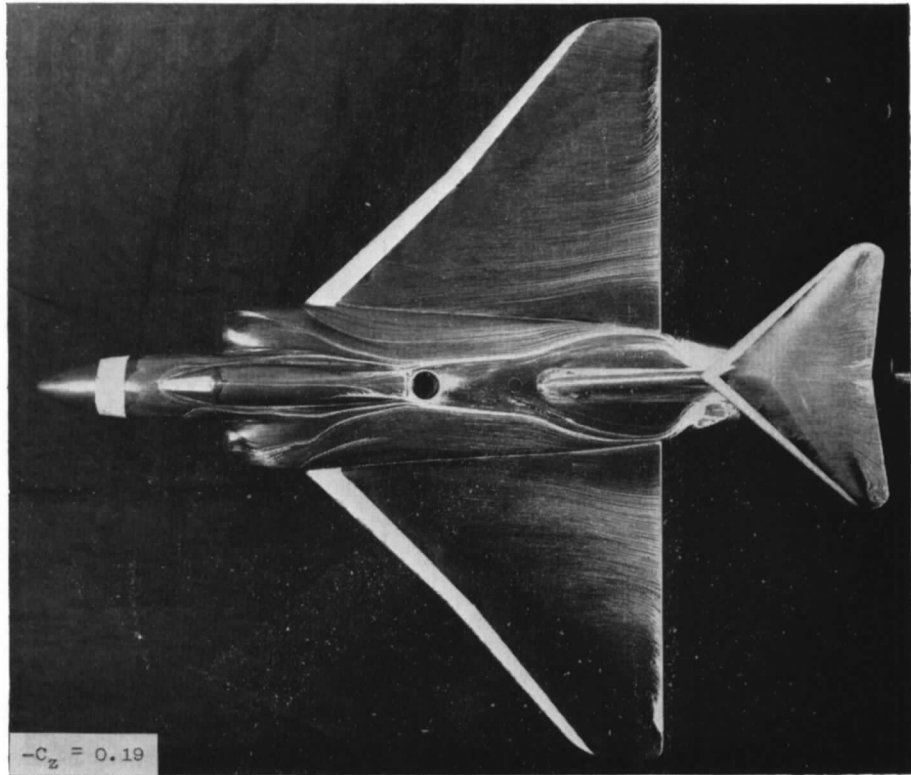
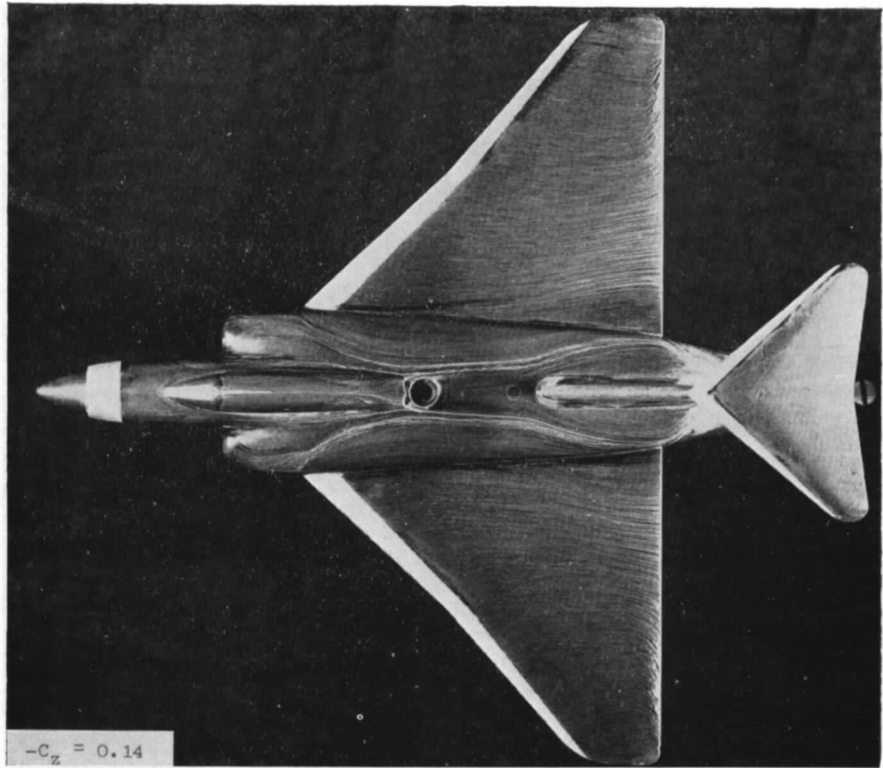


FIG. 39. Oil-flow patterns at $M = 1.00$.

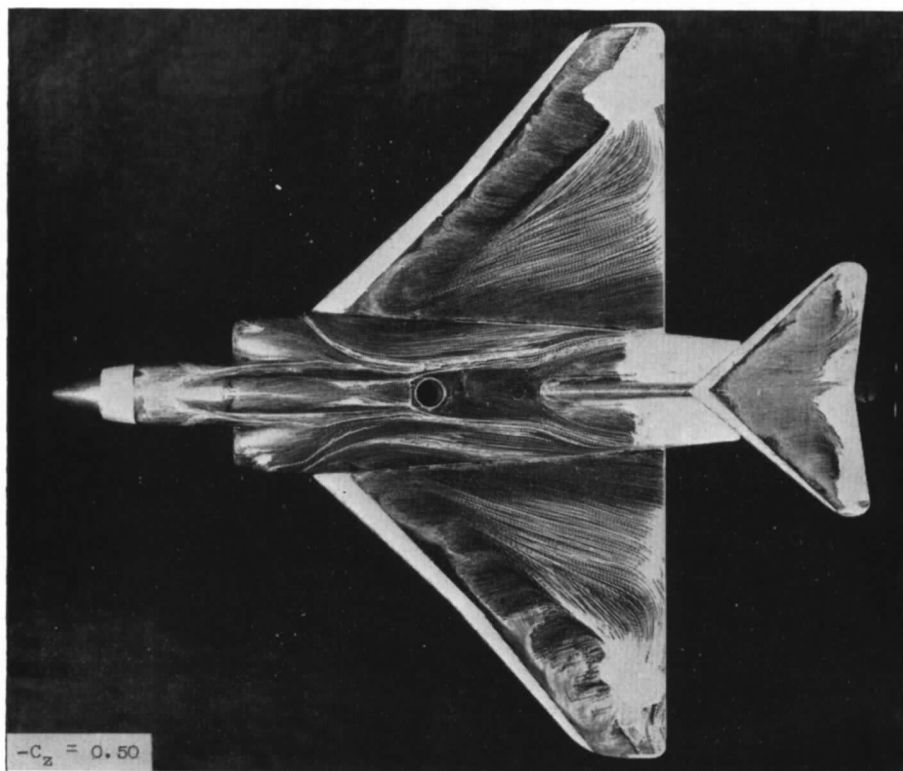
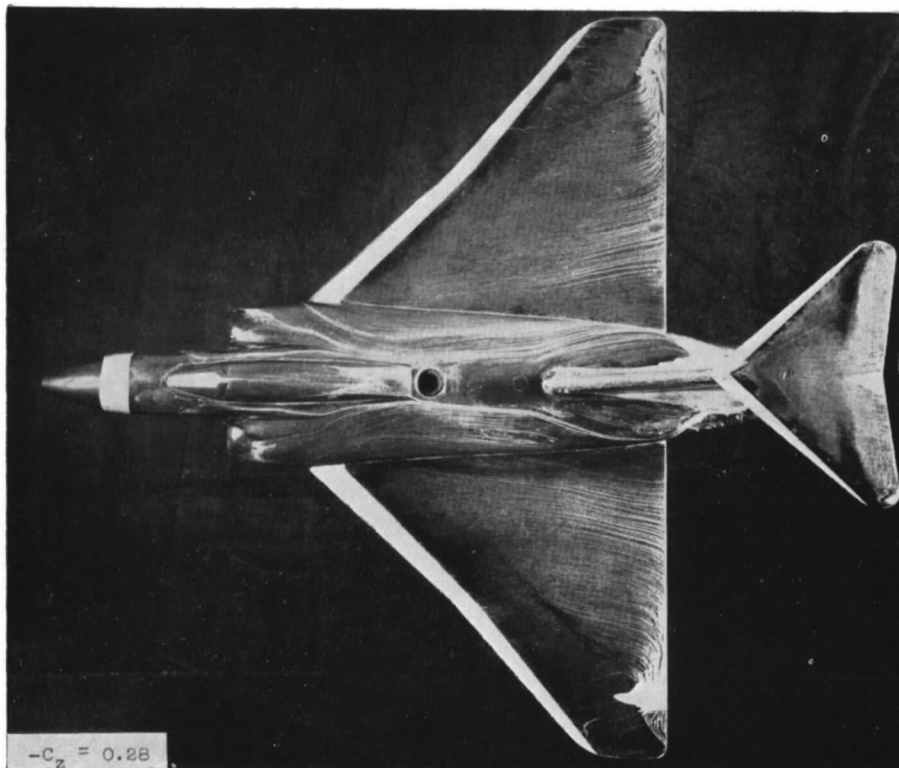


FIG. 39 (continued). Oil-flow patterns at $M = 1.00$.

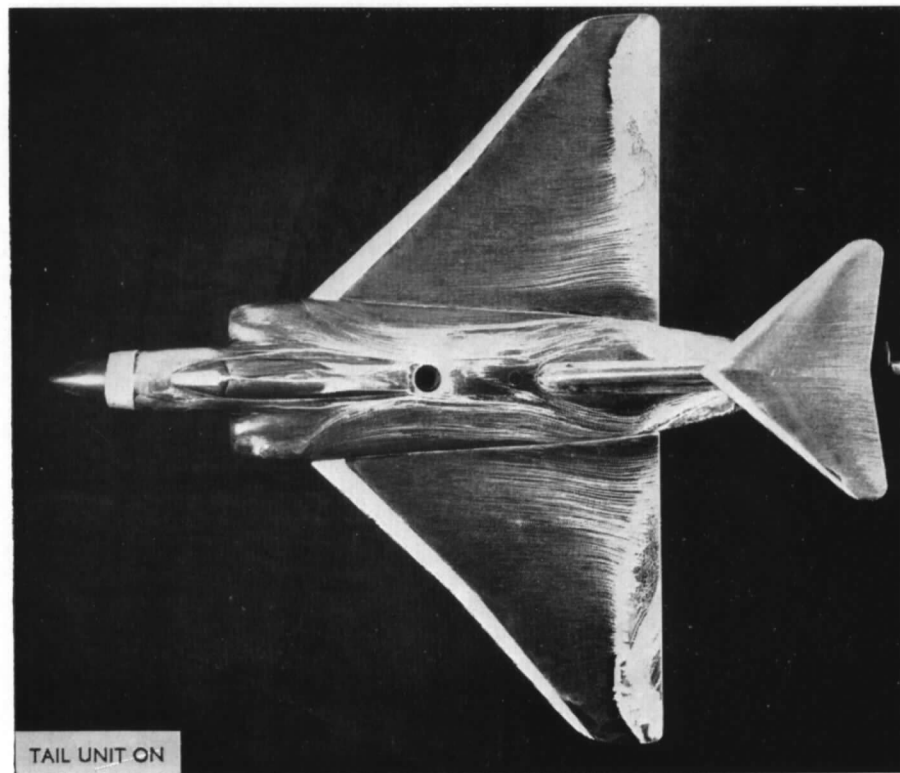
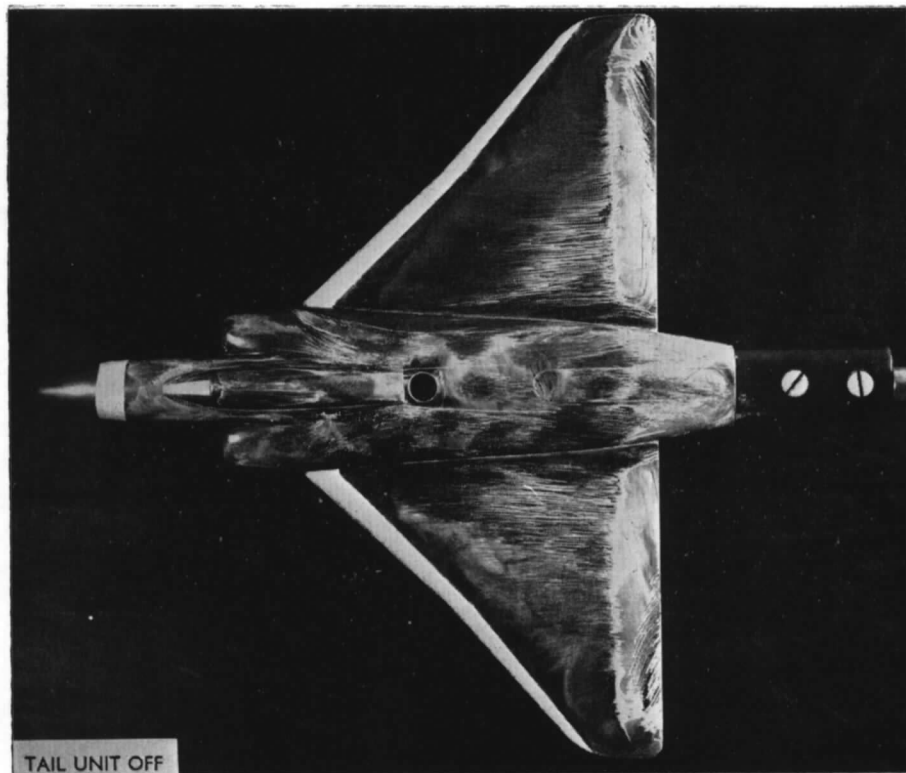
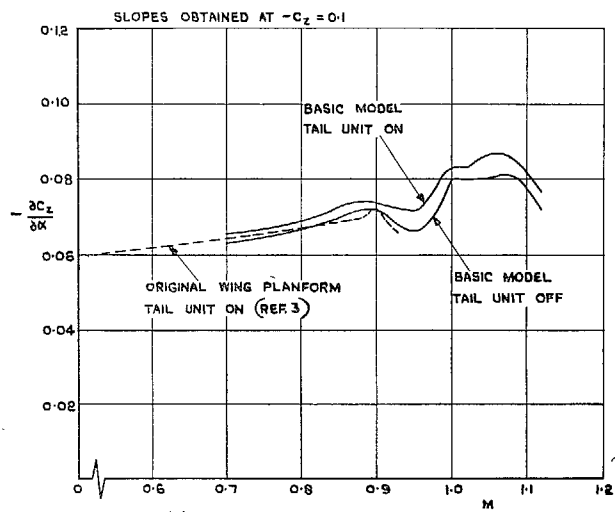
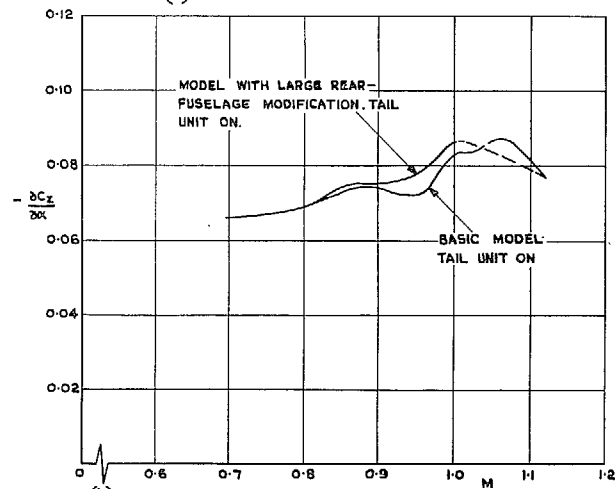


FIG. 40 Effect of presence of tail unit on flow over wing at $M = 0.96$, $-C_z = 0.11$.

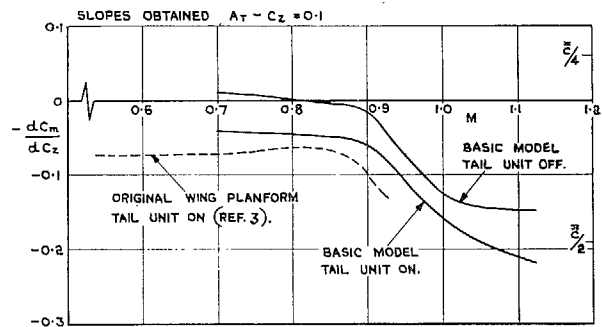


(a) EFFECT OF TAIL UNIT.

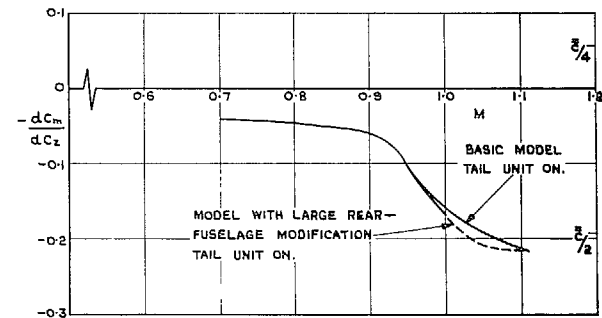


(b) EFFECT OF REAR-FUSELAGE MODIFICATION.

FIG. 41a and b. Variation of $-\partial C_z/\partial \alpha$ with Mach number.



(a) EFFECT OF TAIL UNIT.



(b) EFFECT OF REAR-FUSELAGE MODIFICATION.

FIG. 42a and b. Variation of $-\partial C_m/\partial C_z$ with Mach number.

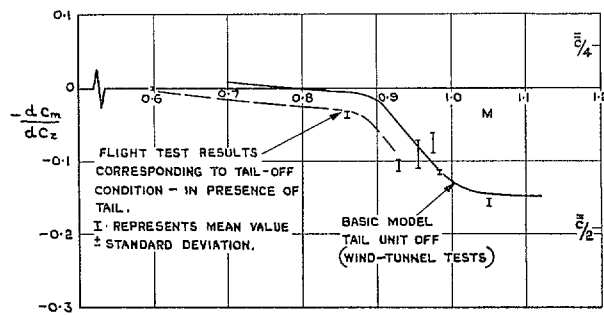


FIG. 43. Comparison of aerodynamic-center positions from tunnel and flight tests.

Publications of the Aeronautical Research Council

ANNUAL TECHNICAL REPORTS OF THE AERONAUTICAL RESEARCH COUNCIL (BOUND VOLUMES)

- 1945 Vol. I. Aero and Hydrodynamics, Aerofoils. £6 10s. (£6 13s. 6d.)
Vol. II. Aircraft, Airscrews, Controls. £6 10s. (£6 13s. 6d.)
Vol. III. Flutter and Vibration, Instruments, Miscellaneous, Parachutes, Plates and Panels, Propulsion. £6 10s. (£6 13s. 6d.)
Vol. IV. Stability, Structures, Wind Tunnels, Wind Tunnel Technique. £6 10s. (£6 13s. 3d.)
- 1946 Vol. I. Accidents, Aerodynamics, Aerofoils and Hydrofoils. £8 8s. (£8 11s. 9d.)
Vol. II. Airscrews, Cabin Cooling, Chemical Hazards, Controls, Flames, Flutter, Helicopters, Instruments and Instrumentation, Interference, Jets, Miscellaneous, Parachutes. £8 8s. (£8 11s. 3d.)
Vol. III. Performance, Propulsion, Seaplanes, Stability, Structures, Wind Tunnels. £8 8s. (£8 11s. 6d.)
- 1947 Vol. I. Aerodynamics, Aerofoils, Aircraft. £8 8s. (£8 11s. 9d.)
Vol. II. Airscrews and Rotors, Controls, Flutter, Materials, Miscellaneous, Parachutes, Propulsion, Seaplanes, Stability, Structures, Take-off and Landing. £8 8s. (£8 11s. 9d.)
- 1948 Vol. I. Aerodynamics, Aerofoils, Aircraft, Airscrews, Controls, Flutter and Vibration, Helicopters, Instruments, Propulsion, Seaplane, Stability, Structures, Wind Tunnels. £6 10s. (£6 13s. 3d.)
Vol. II. Aerodynamics, Aerofoils, Aircraft, Airscrews, Controls, Flutter and Vibration, Helicopters, Instruments, Propulsion, Seaplane, Stability, Structures, Wind Tunnels. £5 10s. (£5 13s. 3d.)
- 1949 Vol. I. Aerodynamics, Aerofoils. £5 10s. (£5 13s. 3d.)
Vol. II. Aircraft, Controls, Flutter and Vibration, Helicopters, Instruments, Materials, Seaplanes, Structures, Wind Tunnels. £5 10s. (£5 13s.)
- 1950 Vol. I. Aerodynamics, Aerofoils, Aircraft. £5 12s. 6d. (£5 16s.)
Vol. II. Apparatus, Flutter and Vibration, Meteorology, Panels, Performance, Rotorcraft, Seaplanes. £4 (£4 3s.)
Vol. III. Stability and Control, Structures, Thermodynamics, Visual Aids, Wind Tunnels. £4 (£4 2s. 9d.)
- 1951 Vol. I. Aerodynamics, Aerofoils. £6 10s. (£6 13s. 3d.)
Vol. II. Compressors and Turbines, Flutter, Instruments, Mathematics, Ropes, Rotorcraft, Stability and Control, Structures, Wind Tunnels. £5 10s. (£5 13s. 3d.)
- 1952 Vol. I. Aerodynamics, Aerofoils. £8 8s. (£8 11s. 3d.)
Vol. II. Aircraft, Bodies, Compressors, Controls, Equipment, Flutter and Oscillation, Rotorcraft, Seaplanes, Structures. £5 10s. (£5 13s.)
- 1953 Vol. I. Aerodynamics, Aerofoils and Wings, Aircraft, Compressors and Turbines, Controls. £6 (£6 3s. 3d.)
Vol. II. Flutter and Oscillation, Gusts, Helicopters, Performance, Seaplanes, Stability, Structures, Thermodynamics, Turbulence. £5 5s. (£5 8s. 3d.)
- 1954 Aero and Hydrodynamics, Aerofoils, Arrestor gear, Compressors and Turbines, Flutter, Materials, Performance, Rotorcraft, Stability and Control, Structures. £7 7s. (£7 10s. 6d.)

Special Volumes

- Vol. I. Aero and Hydrodynamics, Aerofoils, Controls, Flutter, Kites, Parachutes, Performance, Propulsion, Stability. £6 6s. (£6 9s.)
Vol. II. Aero and Hydrodynamics, Aerofoils, Airscrews, Controls, Flutter, Materials, Miscellaneous, Parachutes, Propulsion, Stability, Structures. £7 7s. (£7 10s.)
Vol. III. Aero and Hydrodynamics, Aerofoils, Airscrews, Controls, Flutter, Kites, Miscellaneous, Parachutes, Propulsion, Seaplanes, Stability, Structures, Test Equipment. £9 9s. (£9 12s. 9d.)

Reviews of the Aeronautical Research Council

1949-54 5s. (5s. 5d.)

Index to all Reports and Memoranda published in the Annual Technical Reports

1909-1947

R. & M. 2600 (out of print)

Indexes to the Reports and Memoranda of the Aeronautical Research Council

Between Nos. 2451-2549: R. & M. No. 2550 2s. 6d. (2s. 9d.); Between Nos. 2651-2749: R. & M. No. 2750 2s. 6d. (2s. 9d.); Between Nos. 2751-2849: R. & M. No. 2850 2s. 6d. (2s. 9d.); Between Nos. 2851-2949: R. & M. No. 2950 3s. (3s. 3d.); Between Nos. 2951-3049: R. & M. No. 3050 3s. 6d. (3s. 9d.); Between Nos. 3051-3149: R. & M. No. 3150 3s. 6d. (3s. 9d.); Between Nos. 3151-3249: R. & M. No. 3250 3s. 6d. (3s. 9d.); Between Nos. 3251-3349: R. & M. No. 3350 3s. 6d. (3s. 10d.)

Prices in brackets include postage

Government publications can be purchased over the counter or by post from the Government Bookshops in London, Edinburgh, Cardiff, Belfast, Manchester, Birmingham and Bristol, or through any bookseller

© *Crown copyright* 1965

Printed and published by
HER MAJESTY'S STATIONERY OFFICE

To be purchased from
York House, Kingsway, London w.c.2
423 Oxford Street, London w.1
13A Castle Street, Edinburgh 2
109 St. Mary Street, Cardiff
39 King Street, Manchester 2
50 Fairfax Street, Bristol 1
35 Smallbrook, Ringway, Birmingham 5
80 Chichester Street, Belfast 1
or through any bookseller

Printed in England